Fractures in Complex Fluids: the Case of Transient Networks

Christian LIGOURE · **Serge MORA**

Abstract We present a comprehensive review of the current state of fracture phenomena in transient networks, a wide class of viscoelastic fluids. We will first define what is a fracture in a complex fluid, and recall the main structural and rheological properties of transient networks. Secondly, we review experimental reports on fractures of transient networks in several configurations: shear-induced fractures, fractures in Hele-Shaw cells and fracture in extensional geometries (filament stretching rheometry and pendant drop experiments), including fracture propagation. The tentative extension of the concepts of brittleness and ductility to the fracture mechanisms in transient networks is also discussed. Finally, the different and apparently contradictory theoretical approaches developed to interpret fracture nucleation will be addressed and confronted to experimental results. Rationalized criteria to discriminate the relevance of these different models will be proposed.

Keywords Fracture · transient networks · gels · Non-linear viscoelasticity · complex fluids · brittleness · ductility · fracture nucleation · fracture propagation;

PACS 83.80.Kn · PACS 83.85.Cg · 83.60.Df · 62.20.Mk · 62.20.Fe

C. Ligoure
Laboratoire Charles Coulomb - UMR 5221
Université Montpellier 2 and CNRS
Place E. Bataillon. F-34095 Montpellier Cedex, France E-mail: christian.ligoure@univ-montp2.fr

S. Mora
Laboratoire Charles Coulomb - UMR 5221
Université Montpellier 2 and CNRS
Place E. Bataillon. F-34095 Montpellier Cedex, France E-mail: serge.mora@univ-montp2.fr

List of symbols

G_0	shear modulus
τ	relaxation time
η	viscosity
γ	shear strain
$\dot{\gamma}$	shear rate
$\dot{\varepsilon}$	elongational strain rate
σ	stress
σ_{xy}	shear stress
N_1 or σ_N	First normal stresses difference
W	Griffith energy cost
L	crack size
L_c	Griffith length
F_s	interfacial cohesive energy per unit area
t_b	delay (waiting) fracture time
$\langle t_1 \rangle$	average delay (waiting) fracture time predicted by the *Thermally activated crack nucleation model*
$\langle t_2 \rangle$	average delay (waiting) fracture time predicted by the *Activated bond rupture model*
$\langle t_3 \rangle$	average delay (waiting) fracture time predicted by the *Self healing and activated bond rupture nucleation model*
σ_c	failure stress
σ_1	characteristic stress involved in the *Thermally activated crack nucleation model*
σ_2	characteristic stress involved in the *Activated bond rupture model*
σ_3	characteristic stress involved in the *Self healing and activated bond rupture nucleation model*
$\mathscr{G}$	strain energy release
V	tip velocity
k_B	Boltzmann constant
T	temperature
ξ	typical distance between junctions in a network
ρ	density
Q	injection rate
δ	length of a solvophobic end
De	Deborah number
Γ	Interfacial or surface tension

1 Introduction

The ability of viscoelastic fluids to fracture has been recognized in the sixties [Hutton (1963)] but remains much less documented that the breakdown of solid materials. The starting point for discussing fracture in viscoelastic fluids is coming up with a rigorous definition of fracture. The layman's definition of failure proposed for solid materials by Buehler [Buehler (2010)] - *failure occurs when the load bearing capacity of the material under consideration is significantly reduced or completely lost due to a sudden development* - is not applicable for fluids, which accommodate arbitrarily large deformations after a finite time. At a more fundamental level Buehler argues that fracture of a material due to mechanical deformation can be understood as con-

version of elastic energy into breaking of chemical bonds or heat. This definition is more appropriate for fluids but does not allow to discriminate clearly the fragmentation of liquids due to some hydrodynamic instability [Eggers and Villermaux (2008)] and the fracture of fluids reminiscent of the fracture of solids. For instance, liquid jets serve as a paradigm for hydrodynamic instability leading to drop breakup through the Rayleigh-Plateau capillary instability: in this case, intermolecular (elastic) energy is converted at the surface vicinity alone. A tentative definition for the fracture of fluid could be the following:" the fracture of a fluid due to mechanical deformation, including flow, can be understood as a dissipation of *bulk* elastic energy into breaking of physical or chemical bonds." This definition excludes the hydrodynamic instabilities observed also in inviscid or Newtonian fluids of the field of fluid's fracture because elastic energy that come in play is of interfacial nature solely.

Complex fluids denotes a (too) huge class of condensed-phase materials that posses mechanical properties intermediate between ordinary liquids and ordinary solids [Larson (1999)]. Many of them are "solids" at short time and "liquid "at long time, hence they are *viscoelastic*; the characteristic time required of them to change from "solid" to "liquid" varies from fractions of a second to hours. Numerous extensive studies on the rupture of entangled polymer melts in extension have been carried out in the past forty years. This allows to distinguish two zones of either viscoelastic rupture or elastic fracture in the Malkin-Petrie master curve intended to illustrate the different extensional responses with increasing strain rates of entangled polymer melts [Malkin and Petrie (1997)]. These two types of rupture have been recently reconsidered by Wang [Wang and Wang (2010)]: a yield-to-rupture failure transition is observed: the yield failure (called also ductile failure by other authors [Ide and White (1976, 1977, 1978)] should be due to the yielding of entanglements, whereas at higher extensional strain rates, the specimen breaks up in a purely elastic regime (without any flow).

Among visoelastic fluids, self-assembled transient networks, that consists of reversibly cross-linked polymers in solutions constitute model systems for the physicist, with well defined structural properties and simple linear rheological behavior. The aim of this review is to embrace the current aspects of the phenomenology of transient network's fractures in a compressive manner. We first present what are transient networks: systems and rheology. Second, we report on fracture's experiments and computer simulations of transient networks in several configurations: shear geometry, Hele-Shaw cells and extensional geometry. This also includes, fracture propagation and the extension of the concepts of brittleness and ductility for viscoelastic fluids. Then, we describe the several theoretical approaches developed to describe crack nucleation in transient networks, and how they compare to experiments, before to conclude.

2 Transient networks: systems and rheology

Self-assembled transient (often called physical) networks are a class of complex materials forming spontaneously 3D networks at thermodynamical equilibrium, that can transiently transmit elastic stresses over macroscopic distances. Transient self-

assembled networks are common in both natural and synthetic materials. They consist of reversibly cross-linked polymers in which weak interactions such as hydrogen bonds, hydrophobic interactions, van der Waals forces, or electrostatic interactions are responsible for cross-links formation. Because of the transient character of the junctions, and so of the thermodynamics equilibrium state of these systems at rest, they don't exhibit any aging nor yield stress contrary to other classes of soft out-of-thermodynamic equilibrium viscoelastic materials like dense particulate suspensions (colloidal glasses), or thermoreversible gels [Larson (1999)]. One of the major issue of transient polymer networks is to convey useful rheological properties to solutions, such as increased viscosity, gelation, shear-thinning or shear-thickening. They can be used as controlled drug delivery systems [Sutter et al (2007)], rheological regulators in polymer blends [Kim et al (2004)], coatings, food, and cosmetics, or as matrix materials for tissue engineering [Kim and Mooney (1998)]. Self-assembled transient networks consist mostly of binary solutions of associative polymers, or ternary solutions of associative polymers and self-assembled surfactant aggregates even if supramolecular reversible networks formed by mixtures of small molecules associating by directional interactions has been also reported [Cordier et al (2008)]. Associating polymers are macromolecules with a part that is soluble in a selective solvent (often water), the so-called backbone or spacer to which two or more moieties that do not dissolve in this solvent, the stickers, are attached. The stickers may be randomly distributed along the backbone or may be grouped in blocks. the association of such polymers in solution has been studied extensively, and many reviews can be found in the literature, see for example [Larson (1999); Winnik and Yekta (1997); Berret et al (1997); Meng and Russel (2006); Chassenieux et al (2011)]. Note that the restrictive definition of transient networks that we propose, excludes simple entangled normal or living polymer solutions and melts, where entanglements of polymer chains play the role of transient cross-links and exhibit elastic yielding [Malkin and Petrie (1997); Boukany et al (2009)]. Telechelic polymers are often used as model linkers because they are architecturally simple: they consist of a long solvophilic mid-block with each end terminated by a solvophobic short chain (a sticker) [Semenov et al (1995)]. The stickers incorporate into the solvophobic domains of the aggregates and can bridge them via their solvent-soluble mid-block resulting in an attractive interaction between the aggregates. . The nature and the morphologies of the aggregates forming the network's junctions are versatile: (i) telechelic polymers in binary solution that self-assemble spontaneously into non-interacting flower-like micelles at low concentration and form three dimensional networks above a percolation concentration [Annable et al (1993); Serero et al (2000); Werten et al (2009); Seitz et al (2006)], (ii) surfactant vesicles [Lee et al (2005)], (iii) lyotropic lamellar phases [Warriner et al (1997)] (iv) wormlike micelles [Ramos and Ligoure (2007); Lodge et al (2007); Nakaya-Yaegashi et al (2008); Tixier et al (2010)], (v) spherical micelles [Appell et al (1998); Tixier et al (2010)], (vi) oil-in-water [BaggerJorgensen et al (1997); Filali et al (1999)] or (vii) water-in-oil microemulsion droplets [Odenwald et al (1995)], (viii) photocrosslinkable nano-emulsions [Helgeson et al (2012)].

The rheology of transient networks is determined by the amount and the life time of the bridges. In the simplest case when the bridging chains are flexible and untangled, each bridging chain contributes about 1 $k_B T$ per unit volume to the elas-

tic modulus G_0 according to the theory of rubber elasticity [Green and Tobolsky (1946); Tanaka and Edwards (1992e); Yamamoto (1956)]. The typical value of the shear modulus for these networks ranges between few Pa to several ten thousands Pa. The elastic response relaxes when the solvophobic blocks escape from the core. Often the escape is characterized by a single relaxation time so that the terminal relaxation of the viscoelastic properties is characterized by a single Maxwell process well separated from the faster internal modes that characterize the conformational relaxation of the chains [Annable et al (1993); Serero et al (2000); Michel et al (2000); Filali et al (2001); Tabuteau et al (2009a); Hough and Ou-Yang (2006)]. Far above the percolation concentration, the viscoelastic relaxation time τ is related to the average lifetime of a connection [Green and Tobolsky (1946)] which in turn depends on the breakage probability of a cross-link. The average lifetime of bridge will depend on its chemical nature, the external conditions and the physical state of the cross-links. It can vary through few ms [Tixier et al (2010)], few seconds [Michel et al (2000); Filali et al (2001)], up to hours [Serero et al (2000); Skrzeszewska et al (2010); Seitz et al (2006)]. The simplicity of the linear viscoelastic behavior of most of self-assembled transient networks is in contrast with their highly complex non-linear response that can vary widely [Pellens et al (2004b)]. Among all systems, the experimental model transient network consisting of oil-in-water microemulsion droplets reversibly linked by telechelic polymers [Filali et al (2001); Michel et al (2000)] is perhaps the unique one which exhibits the steady shear flow curve of a pure Maxwell fluid for both the shear stress and the first normal stress difference until it breaks [Tabuteau et al (2009a)]. In most other systems, the steady shear viscosity exhibits three flow regimes. Above a Newtonian plateau (linear regime), the viscosity increases considerably (shear thickening) prior to the onset of shear thinning at higher shear rates [Annable et al (1993); Xu et al (1996); Otsubo (1999); Berret and Serero (2001); Pellens et al (2004a); Tripathi et al (2006)]. However, the shear thickening region is not always present [Michel et al (2000); Tixier et al (2010); Tirtaatmajda and Jenkins (1997); Mewis et al (2001); Skrzeszewska et al (2010)]. A large number of constitutive theoretical models are based on the temporary-network kinetic model for telechelic polymers network theory [Tanaka and Edwards (1992e)] by applying the original ideas formulated by Green and Tobolsky [Green and Tobolsky (1946)] and Yamamoto [Yamamoto (1956)] and have been developed to tentatively capture the main features of non-linear rheological properties of these networks [Marrucci et al (1993); Ahn and Osaki (1995); van den Brule and Hoogerbrugge (2000); Vaccaro and Marrucci (2000); Tripathi et al (2006); Hernandez-Cifre et al (2003)].

3 Fracture experiments

Several geometries have been considered to explore fracture mechanisms in transient networks: elongational flows using either extensional rheometer [Tripathi et al (2006)], pendant drop experiments [Tabuteau et al (2009a, 2011)], shear flows in rheometric cells [Berret and Serero (2001); Tabuteau et al (2009a); Tixier et al (2010); Skrzeszewska et al (2010)] or flows in Hele-Shaw cells [Zhao and Maher (1993); Ignés-Mullol et al (1995); Vlad et al (1999); Mora and Manna (2010)].
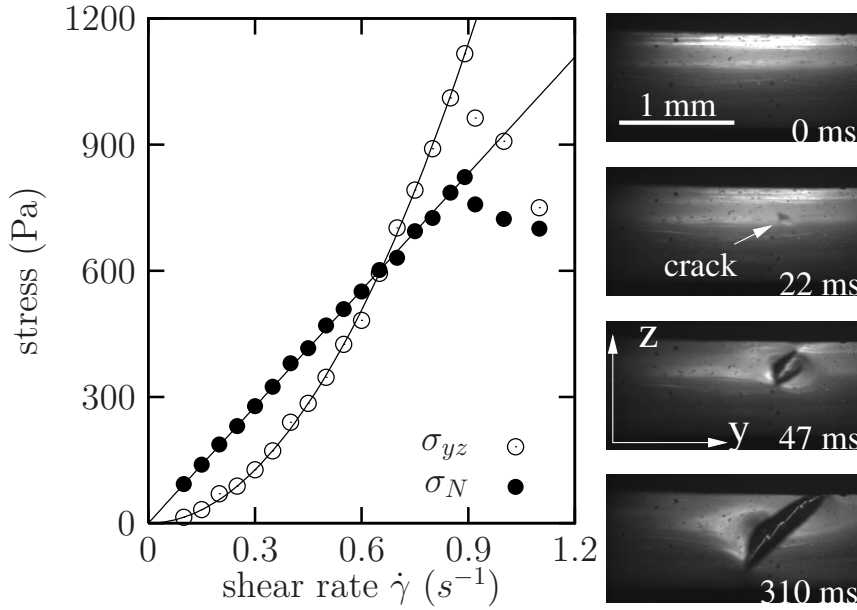
Fig. 1 From [Tabuteau et al (2009a)]: **(Left)** shear stress (σ_{yz}) and first normal stresses difference ($\sigma_N = \sigma_{zz} - \sigma_{yy}$) versus shear rate for a bridged microemulsion with a shear modulus $G_0 = 1210$ *Pa* and a relaxation $\tau = 0.8$ s. The continuous lines are fits (Maxwell model). **(Right)** Development of a fracture, occurring at the surface of the sample, for a shear rate equal to 0.9s^{-1}, corresponding to a critical first normal stresses difference $\sigma_N = 1190$ Pa.

3.1 Shear-induced fractures

3.1.1 Stationary shear rate

When submitted to a constant shear rate $\dot{\gamma}$, the measured shear stress σ_{xy} of "brittle" transient networks first increases smoothly with the shear rate [Molino et al (2000); Berret and Serero (2001); Tabuteau et al (2009a); Skrzeszewska et al (2010); Tixier et al (2010)]. However, above a critical shear rate $\dot{\gamma} \sim \tau^{-1}$, where τ is the relaxation time of the network, the flow curve exhibits a sharp discontinuity (Figure 1) and the viscosity decreases abruptly. Below this value, the branch of the flow curve can be Newtonian and shear thickening [Berret and Serero (2001)], or only Newtonian [Molino et al (2000); Tabuteau et al (2009a); Skrzeszewska et al (2010)], or Newtonian and shear thinning [Tixier et al (2010)] depending on the experimental system under consideration. Note that for "brittle "transient networks, the first normal stresses difference $N_1 = \sigma_{xx} - \sigma_{yy}$ drops suddenly for the same critical shear stress [Tabuteau et al (2009a)]. Authors of [Molino et al (2000)] were the first to suggest that the sudden drop of the stress in the flow curve of a transient network is the sign of a fracture propagation.

However, the first unambiguous demonstration of shear-induced fractures in transient networks was done in [Berret and Serero (2001)], by using a flow visualization technique in a plate-plate transparent shearing cell. At low shear rate, the velocity

profile is homogeneous: the velocity decreases linearly from the rotating wall to the stationary one. Above the critical shear rate, the stationary velocity field within the gap of the cell exhibits a discontinuity, that defines a zone of fracture as the part of the fluid submitted to a high shear rate ($\sim$ 10 times the applied rate). This has been confirmed by Skrzeszewska *et al* [Skrzeszewska et al (2010)] by Particle Image Velocimetry: the fracture zone has an irregular shape and is rather wide on the order of a few hundred micrometers. With increasing overall shear rate, the width of the fracture zone increases. The fracture zone can happen everywhere in the gap and is different for every experiment. For non-adhesive gels, the fracture zone occurs generally at one of the wall [Berret and Serero (2001)], and so appears as sliding, that is observed in other classes of complex fluids like pastes or concentrated emulsions [Meeker et al (2004)], whereas for adhesive gels [Skrzeszewska et al (2010)], or rough wall surfaces [Tixier et al (2010)], the fracture occurs in the bulk. A direct optical observation of the shear fractures [Tabuteau et al (2009a)] shows that above the critical stress, cracks open up all around the sample and grow rapidly. It is worth noting that the fractures are tilted $45°$ from the shear plane, perpendicular to the direction of the maximum extension (Figure 1). Interestingly, for two very different systems [Tabuteau et al (2009a); Skrzeszewska et al (2010)] that have perfectly Newtonian flow curve, before fracture occurs, the fracture shear stress in the steady state flow curve scales as $\sigma_{xy} \sim G_0$, where G_0 is the shear modulus of the network. In contrast to solids, here the fractures heal over rapidly after the shear rate is switched off, and a new experiment can be performed after a few minutes with quantitatively the same behavior [Tabuteau et al (2009a); Skrzeszewska et al (2010)].

Above the critical fracture shear rate, strong fluctuations of the shear stress have been observed [Sprakel et al (2009a); Tixier et al (2010); Ramos et al (2011)], that can lead to an apparent shear plateau [Sprakel et al (2009a)] reminiscent of shear-banded flows observed in a wide variety of soft materials such as solutions of entangled wormlike micelles, colloidal suspensions and entangled polymer solutions [Fielding (2007); Olmsted (2008)]. Such strong fluctuations of the shear stress have also been observed in solutions of entangled wormlike micelles at high shear rate and have been associated also with a rupture-like behavior as evidenced by Particle Tracking Velocimetry [Boukany and Wang (2007)]. By using a novel class of transient networks made of surfactant micelles of tunable morphology [Tixier et al (2010)] (from spheres to rods to flexible worms) linked by telechelic polymers, and coupling rheology and time-resolved structural measurements, Ramos and Ligoure [Ramos et al (2011)] clearly show that true shear-banding is *not* associated with strong fluctuations of the shear stress. Indeed, fluctuations of the shear stress are entirely correlated to the fluctuations of the degree of alignment of the micelles that can probe a fracture process. Sprakel *et al* [Sprakel et al (2009a)] argue that the intermittent behavior observed in the stress response is due to repeated microfracture-healing events in the material. The cumulative distribution of the total stress drops $\Delta\sigma$ during a fracture displays a characteristic power-law behavior, $\mathscr{P}(>\Delta\sigma) \propto \delta\sigma^{-0.85}$, with $\mathscr{P}$ the stress probability distribution. The exponent is close to the value of 0.8 reported for true stick-slip motion [Feder and Feder (1991)]. Attempts to explain such scaling behavior involve the concept of self-organized criticality.
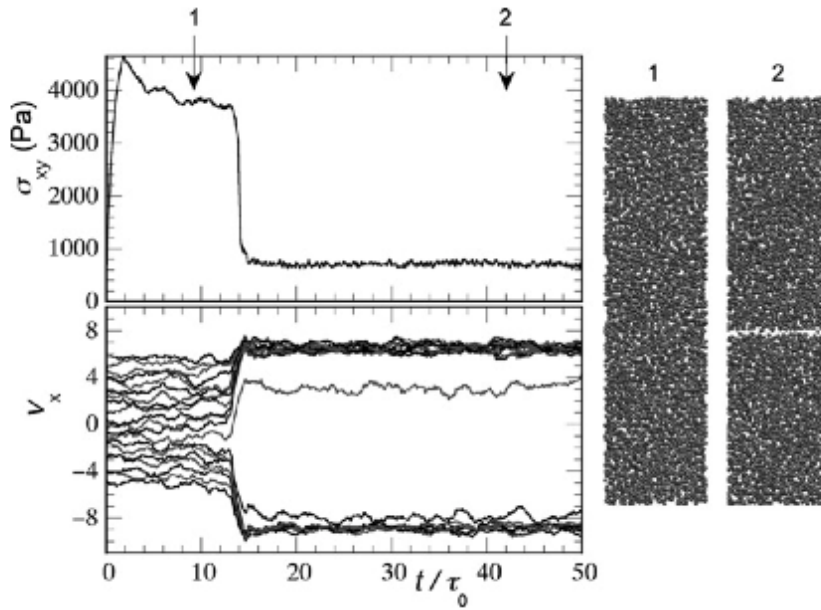
Fig. 2 From [Sprakel et al (2009b)]: Transient shear stress response in a shear start-up run. Bottom panel shows the corresponding evolution of the velocity profile, in which each line represents the local fluid velocity $(v_x(y,t))$ at a given position in the gradient direction. Snapshots of the simulation box (flow from left-right with a velocity gradient from top-bottom) illustrate the homogeneous initial configuration (left) and the final fractured state (right).

Responsive particle dynamics simulations [Sprakel et al (2009b)] have also shown shear-induced fractures (Figure 2) in transient polymer networks. Moreover these simulations have revealed a transition from shear banding to fracture upon increasing the overall polymer concentration. and emphasize the difficulty to define an unambiguous criterion to discriminate between banding and fracture. In the literature, banding is usually defined as situations where the velocity profile in the gradient direction is continuous but kinked, whereas it is discontinuous at the plane of fracture. It is worth mentioning than the the issue of velocity change within the gap is in fact more complicated [Manneville (2008)] in addition to "classic banding" coexistence of yielded and unyielded regions with finite and zero rates/velocities have been observed in systems like colloidal glasses [Besseling et al (2010)]. Unfortunately the spatial accuracy is typically limited to the micrometer range and cannot allow to distinguish between narrow high shear bands and fracture planes. However the authors of [Sprakel et al (2009b)] show that a discontinuity in the variation of the first normal stresses difference N_1 with the shear-rate is an unambiguous signature of a fracture, since normal forces should be largely reduced as all connections between the two shear bands across a fracture plane are broken. The discontinuity of N_1 at the threshold has been observed experimentally for fracturing transient networks [Tabuteau et al (2009a); Tixier et al (2010)], in contrast with shear-banding regimes [Tixier et al (2010)], where N_1 increases with $\dot{\gamma}$ as expected theoretically [Spenley et al (1993)].

3.1.2 Fracture at constant applied stress

Another approach to study the failure of gels is to apply a constant stress and to follow the resulting shear rate as a function of time [Skrzeszewska et al (2010)]. Above the critical fracture stress $\sigma \sim G_0$, fracture occurs immediately as revealed by a dramatic increase of the measured share rate. Below the critical fracture shear stress, a delayed time is observed before fracturing, a phenomenon well documented in solid materials [Zhurkov (1965); Santucci et al (2007)] and observed also in colloidal suspensions [Sprakel et al (2011); Divoux et al (2010)], wormlike micelles [Olsson et al (2010)] and soft elastomers [Bonn et al (1998)]. The delay fracture time t_b varies significantly from one experiment to an other one indicating the stochastic nature of the fracture mechanism. With decreasing stress, the average delay time increases $< t_b >$ rapidly. Several theoretical interpretations have been proposed, that will be reviewed in Section 5). They predict different delay fracture times. However, the intrinsic stochastic nature of the fracture mechanism implies a very large uncertainty of $< t_b >$ that does not allow to conclude definitively about the relevant theory.
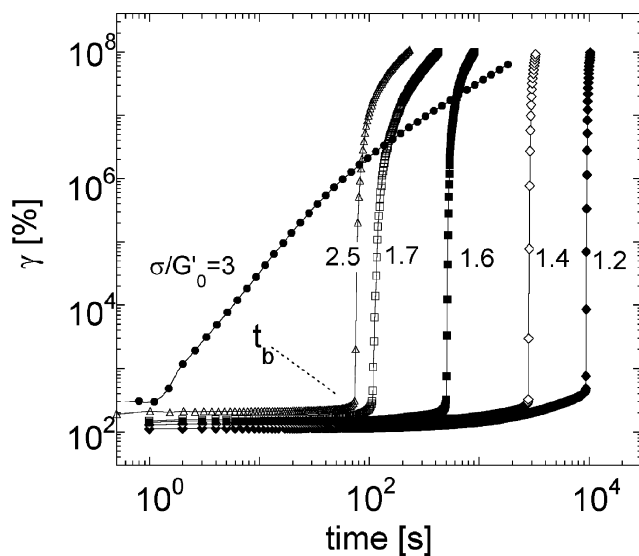
Fig. 3 From [Skrzeszewska et al (2010)]: Delayed fracture of a transient polymer network formed by telechelic polypeptides, for different applied stresses. After a certain waiting time which varies from one experiment to another, the gel breaks, leading to a very rapid increase of the overall strain.

3.2 Fractures in Hele-Shaw cells

Fracture-like flow instabilities that arise when a fluid is injected into a Hele-Shaw cell filled with an aqueous solution of telechelic polymers has been reported by several authors [Zhao and Maher (1993); Ignés-Mullol et al (1995); Vlad et al (1999);
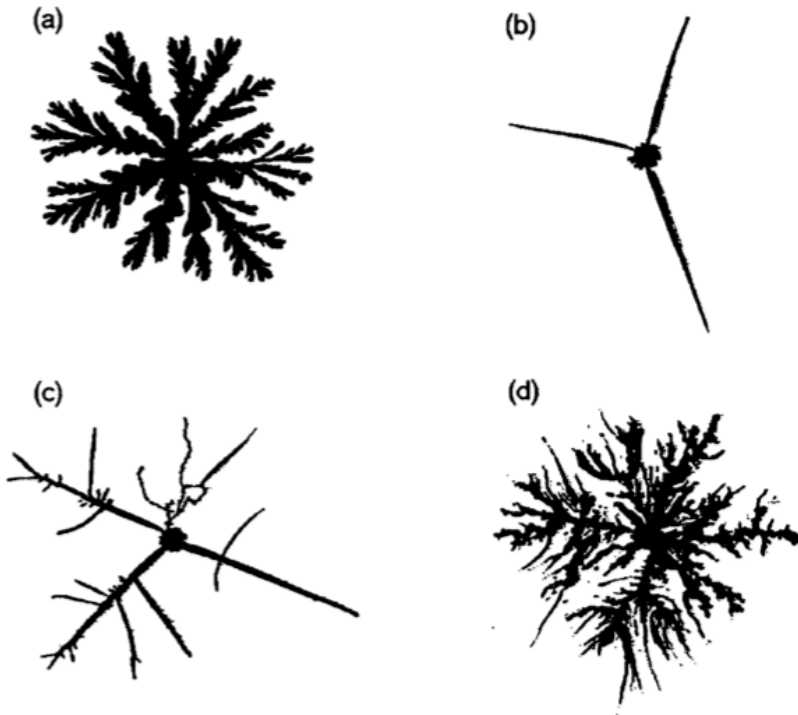
Fig. 4 From [Zhao and Maher (1993)]: Four typical patterns of a 2.5% solution of hexadecyl end-capped polymers of molecular weight 50 700 at injection rates (a)$Q = 1.0$ mL/min, (b) $Q = 1.0$mL/min, (c) $Q = 5.0$ mL/min, and (d) $Q = 20$ mL/min. The crossover from the viscous-fingering pattern to the fracturing pattern is seen in (a) and (b).

Mora and Manna (2010)]. Zhao and Maher [Zhao and Maher (1993)] showed using a radial Hele-Shaw cell, that for transient networks of associative polymers, there exists a threshold injection rate, below which the pattern instability is typically viscous fingering (Saffman-Taylor instability) [Bensimon et al (1986)], and beyond which, the patterns resemble fracture patterns observed in brittle materials (Figure 4). Note that analogous fracture patterns have been also observed in other classes of complex fluids like clay suspensions [Lemaire et al (1991)] or lyotropic lamellar phases [Greffier et al (1998)]. The difference between a fingering pattern and a fracture pattern is drastic and can be quantified by calculating the mass fractal dimension of a given pattern: it drops drastically from ~ 1.70 to ~ 1.0 near the transition threshold. Interestingly, the fingering/fracture transition is not observed for the corresponding entangled homopolymers solutions, indicating that the fingering-fracturing transition is a direct manifestation of an associating-network effect. A characteristic, Deborah number $D_e = \tau_{thin}/\tau_f \sim (\tau Q)/(b^2 L_{cell})$ can be defined, where $\tau_{thin} = 1/\dot{\gamma}_{thin}$ is the inverse of the shear thinning rate of the transient network and *not* its relaxation time τ, Q is the injection rate, b the thickness of the cell and L_{cell}, some characteristic length scale of the radial cell. The transition from fingering to fracture-like behavior
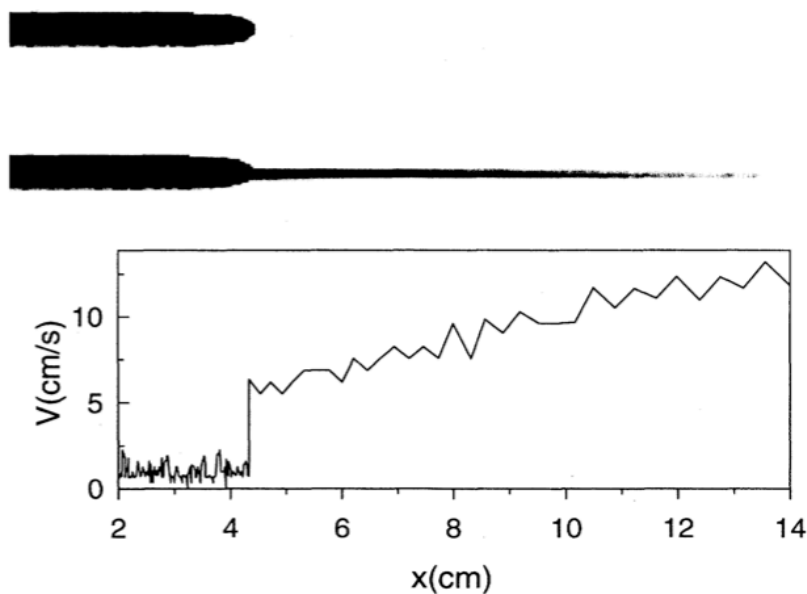
Fig. 5 From [Ignés-Mullol et al (1995)]: Fracture involving an associative polymer polymer of molecular weight 17400. **Top**: viscous finger at early times. The shape is that of a Saffman- Taylor finger. **Middle**: the fracture-like pattern emerges cleanly from the unperturbed finger. **Bottom**: tip velocity as a function of tip position during the growth).

appeared roughly at the same Deborah number under variation of polymer molecular weight or polymer concentration.

Dynamics fracture-like flows instabilities of associating polymers solutions has been also characterized in a rectangular Hell-shaw cell by measuring the crack tip velocity [Ignés-Mullol et al (1995)] or the tip mobility which relates the velocity of the tip to the pressure gradient [Vlad et al (1999)]. The resulting pattern of the flow instability is highly dependent on the concentration, molecular weight or architecture of the associative polymer solutions. For low molecular weight polymer, the onset of fracture-like pattern evolution is accompanied by an abrupt jump in the tip velocity followed by a constant low acceleration (Figure 5). At high molecular weight, the transition is blurred by a meandering regime in which the crack tip meanders from side to side and fluctuates with a characteristic frequency proportional proportional to the fluid injection rate.

Mora and Manna [Mora and Manna (2009, 2010, 2012)] revisited both theoretically and experimentally the Saffman-Taylor instability for a model viscoelastic fluid, i.e. a upper-convected Maxwell fluid, a versatile experimental realization of which consisting a transient network of oil in water microemulsion droplets droplets reversibly linked by telechelic polymers [Filali et al (1999)]. They prove [Mora and Manna (2010)] that a unique dimensionless parameter $\tilde{\tau} = \frac{b^2(-\nabla P)^{3/2}}{G_0 \Gamma^{1/2}}$ (b is the thickness of there Hele-Shaw cell, ∇P is the applied pressure gradient, Γ, the surface
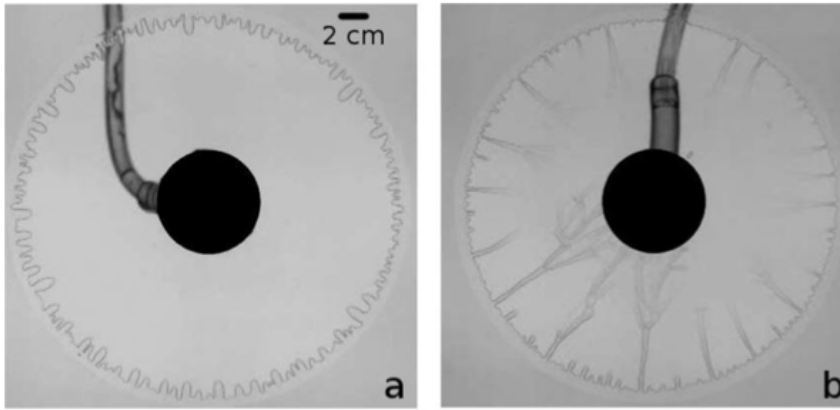
Fig. 6 From [Mora (2011)]: Aspiration of a Maxwell fluid in a radial Hele-Shaw cell: (a) Elastic pattern formation for $\tilde{\tau} = 5$, (b) Fracture-like pattern for $\tilde{\tau} > 10$.

tension of the network and G_0 is the zero shear modulus), controls all elastic effects and particularly, the fracture transition. Note that $\tilde{\tau}$ does not depend on the fluid viscosity but on the elastic modulus. The theory describes the transition from viscous to elastic fingering instability and shows that there is a divergence of the maximum growth ratio of the instability, which occurs for a finite value of the control parameter $\tilde{\tau} = 10.2$. Experimentally (Figure 6), the main results is the fracture-like pattern observed above a critical value $\tilde{\tau}_c^{exp} \simeq 10$ for every fluid, very close to the predicted theoretical value. So, the fracture is a direct consequence of the predicted blow up and the existence of the fracture-like pattens is a consequence of the elasticity of the complex fluid and takes place within the linear regime.

3.3 Fractures in extensional geometry

3.3.1 Filament stretching rheometry

Extensional properties including fractures of associative polymer networks remain virtually unexplored until the development of filament stretching rheometry [Anna et al (2001); McKinley and Sridhar (2002); Anna and McKinley (2008)]. Tripathi et al. [Tripathi et al (2006)] investigated the non-linear extensional rheology of end-capped urethane coupled poly-(oxyethylene) (HEUR) using a filament stretching rheometer. A nearly cylindrical sample of transient network fills the gap between two rigid circular plates that are moved apart to a final separation with an exponentially increasing separation profile $L(t) = L_0 \exp(\dot{\varepsilon}t)$, where $\dot{\varepsilon}$ is the strain rate, the evolution of the tensile force and mid-filament diameter being measured simultaneously. The authors varied both the polymer concentration and the molecular weight of the polymer. They observed that, for sufficiently low polymer concentration (sufficiently low network strength), and at high strain rates and Deborah number (defined
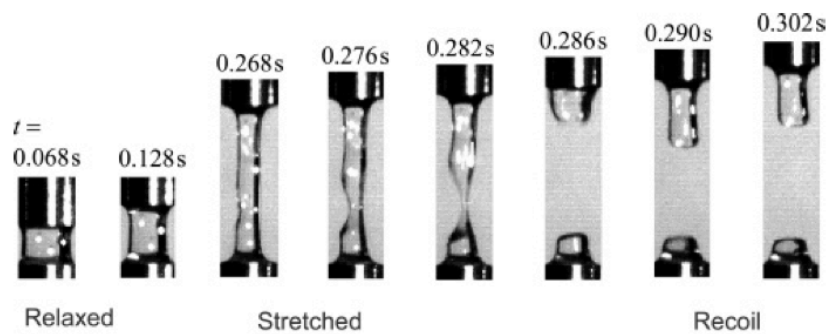
Fig. 7 From [Tripathi et al (2006)]: Images showing rupture of 2.4wt % HEUR22-2, for an applied strain rate $\dot{\varepsilon} = 3 s^{-1}$.

as $De = \tau \dot{\varepsilon}$, where τ is the Maxwellian relaxation time), a defect appears in the filament and a tear propagates rapidly across the filament leading to a complete rupture in two distinct domains followed by an oscillatory damping elastic recoil of the two pieces toward the two end planes (see Figure 7). The failure of the filament occurs before any significant necking has occurred. This type of rupture instability has also been observed in polymer melts [Joshi and Denn (2004)] and entangled solutions of wormlike micelles [Rothstein (2003); Bhardwaj et al (2007)]. At lower Deborah numbers, the fluid filament pinches off through a visco-capillary or elasto-capillary thinning, and occurs after a considerable necking of the filament. These two different rupture scenarios (elastic rupture versus necking and pinch-off) observed in transient networks and more generally in polymeric liquids are reminiscent of brittle versus ductile fracture behaviors [Tabuteau et al (2008)] observed in solid materials, reviewed in section 4.

Tripathi *et al* [Tripathi et al (2006)] interpret the failure behavior of the transient network filaments in the context of the Considère construction [Considère (1885)], originally developed in solid mechanics to quantitatively predict the critical Hencky strain to failure, despite the doubts about its applicability to the prediction of the inception of necking in extensional flow [Petrie (2009)]. The original Considère construction is that, if the graph of force against stretch ratio has a maximum, there is the possibility of two stretch ratios corresponding to the same force, which can be associated with the formation of a neck in the solid sample, leading to the failure. Renardy [Renardy (2004)] noted that fluid threads described by constitutive models in which the extensional viscosity passes through a maximum may undergo a purely elastic mode of necking failure in which surface tension plays no role. The observations of Tripathi et al of filament necking and rupture processes observed experimentally appear to be connected to an instability resulting from saturation in the tensile stresses at a critical deformation rate. It has been associated with a maximum in the extensional viscosity as a function of rate of strain in the constitutive rheological model used to described transient networks, so that this maximum of extensional viscosity is claimed to be an analogue for liquids of the Considère criterion for solids. However, such an analogy to interpret the failure of transient networks requires great care

and at worst leads to confusion and misleading conclusions as developed in the review of Petrie [Petrie (2009)], due to the use of too crude constitutive models for the complex fluids and a strong dependence on the details of the extensional flow. Recently, Fielding [Fielding (2011)] finds, contrary to the Considère criterion, the onset of instability to relate closely to the onset of downward curvature in the time (and so strain) evolution of the z component of the molecular strain, for extension along the z axis.

3.3.2 Fracture of pendant drops

The fall and failure of a viscous fluid droplet from a faucet has been extensively studied both experimentally an d theoretically (see the reviews by Eggers and Villermaux [Eggers and Villermaux (2008)] and Eggers [Eggers (1997)]). However, for non-Newtonian fluids, such a surface free flow lead to highly non-linear fluid motion, in particular strong stretching that are usually non-well tested by Non-Newtonian constitutive laws, and few quantitative experiments have been available. Smolka and Belmonte [Smolka and Belmonte (2003)] reported the filament dynamics and rupture of pendant drops of viscoelastic wormlike micellar fluids: the rupture is consecutive of a necking and pinching off instability followed by a partial retract of the free filament ends, is also reminiscent of a ductile fracture behavior observed at low Deborah numbers in filament stretching rheometry experiments performed on transient networks [Tripathi et al (2006)].

The single report (to the best of our knowledge) of fail and rupture of pendant drops of transient network has been done by Tabuteau *et al* [Tabuteau et al (2009a)]. The experimental system they used is a model network consisting of oil in water microemulsion droplets linked by telechelic polymers (described in section 2), which has the peculiarity to exhibit a pure linear Maxwell behavior as long as it flows. A drop emerges at a constant rate of 2mL/h from a plastic tube of 2.6 mm diameter. The drop of fluid begins to fall when its weight exceeds the surface tension retaining force; a filament is formed and stretched by the failing drop until a crack nucleates somewhere around the filament (Figure 8) and then the fracture propagates perpendicularly to the filament. The total duration of the fall before the opening is typically on the order of 50 to 200 s depending on the sample, much larger than the relaxation time of the fluid ($\sim$ 1s), itself much larger than the total duration of the rupture event ($\sim$ few ms). After that the complete rupture was achieved, an elastic retraction of the remaining pendant piece of the filament is observed. Upon growing, the fracture exhibits a parabolic shape expected for an elastic solid breaking under tension [Greenwood and Johnson (1981); Barenblatt (1962)]. The authors measured the diameter of the drop where the fracture occurs and weighted the mass of the falling part, so they can measure the rupture stress σ_c as a function of the shear modulus of the gel, that can be varied by varying the polymer concentration. Moreover, the authors performed several measurements of the rupture stress of two samples with the same composition (oil mass fraction: 10% and mean number of polymer sticker per droplet: 6) and the same shear modulus $G_0 = 1200$ Pa *but* with two different lengths of the hydrophobic alcane chains constituting the stickers of the telechelic polymers (21 methyl groups and 18 methyl groups respectively). The relaxation time of the
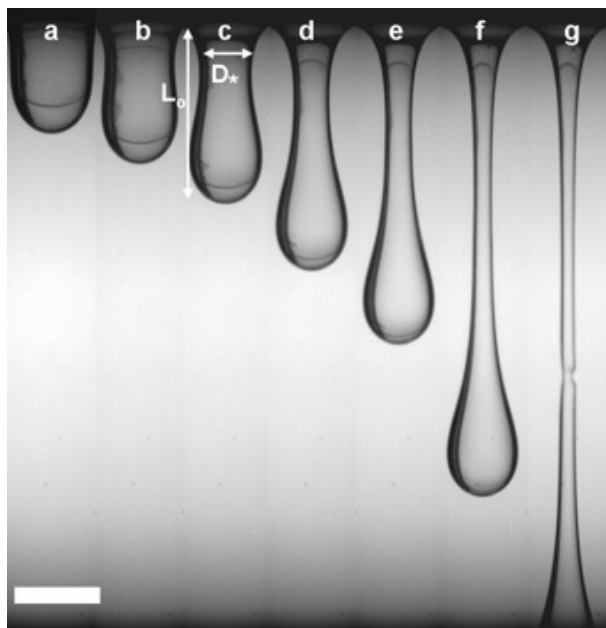
Fig. 8 From [Tabuteau et al (2011)]: Sequence of images of the fall of a drop of a transient network. Regime 1 (drop formation) corresponds to images (a) and (b) and regime 2 (viscous fall) corresponds to images (c) to (g). Image (g) corresponds to the beginning of the brittle fracture regime. At the beginning of regime 2, the radius of the filament is defined as $R* = D*/2$ and L_0* is the length of the drop. The white scale bar corresponds to 2.5 mm.

C_{21} sample is five times larger than the relaxation time of the C_{18} sample. The mean value of the rupture stress is found to be identical for the two samples, with also the same relative standard deviation. This indicates that the rupture stress is *independent* of the binding energy.

An other important point reported in [Tabuteau et al (2009a)] is that the rupture occurs in the linear regime $\sigma_c \approx G_0$, so that the critical rupture stress is close to shear modulus of the network (see Figure 10). The *thermally activated fracture model* developed in section 5.2 allows a quantitative interpretation of these behaviors. One of the key points to understand this mechanism of fracture is the bond reversibility and the corresponding relevant ultra low interfacial energy needed to nucleate the crack. This interfacial tension results from the loss of conformational entropy of polymeric bonds near a crack interface and is typically on the order of few μNm^{-1} [Sprakel et al (2007)]. The origin of this ultra low interfacial tension will be discussed in section 5.2.

3.4 Fracture propagation

The propagation of fractures in transient networks is less documented [Ignés-Mullol et al (1995); Vlad et al (1999); Tabuteau et al (2011)] than in permanent gels, such
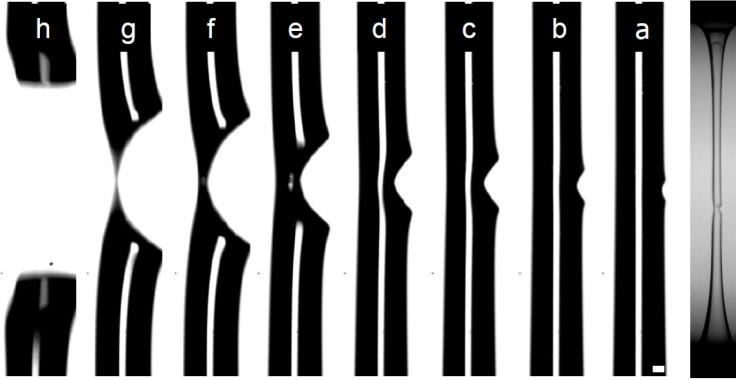
Fig. 9 From [Tabuteau et al (2011)]; Pictures of the propagation of a fracture across a pendant filament of a transient network from the right to the left. The time left to achieve complete fracture of the filament corresponding to each picture labelled with a letter is: a (8.50 ms), b (5.16 ms), c (2.67 ms), d (2.00 ms), e (1.00 ms), f (0.33 ms), g (0.17 ms) and h (0.ms). The last picture on the right shows almost all of the elongated drop, with the crack being well developed. The white scale bar corresponds to 0.1 mm.
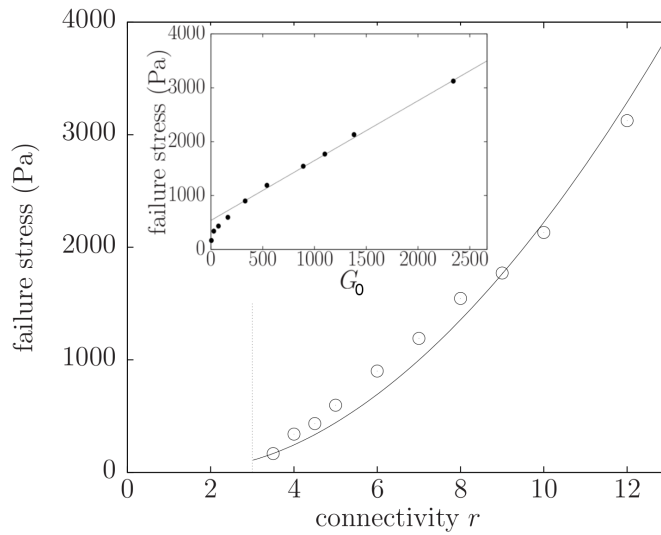
Fig. 10 From [Tabuteau et al (2009a)]: Plot of the rupture stress coming from the pendant drop experiments (σ_b, circles) and the expected values coming from Eq. 7 (σ_1, line) as a function of the connectivity r. The vertical dashed line corresponds to the percolation threshold ($r=3$). The inset gives the variation of the experimental rupture stress with the shear modulus, corresponding to the different connectivity. Note that the observed deviation of σ_1 from its linear dependence with the shear modulus G_0 observed at small r, originates from the vicinity of the percolation threshold [Filali et al (1999)].

as covalent hydrogels [Tanaka et al (2000); Livne et al (2007, 2005)], biopolymer hydrogels (gelatin [Baumberger et al (2006b,a); Baumberger and Ronsin (2010a)] or alginates [Baumberger and Ronsin (2010b, 2009)]) and permanent self-assembled triblock copolymer gels [Seitz et al (2009)]. If one excepts some reports on dynamics fracture of associating polymers in Hele-Shaw cells [Ignés-Mullol et al (1995); Vlad et al (1999)] already reviewed in section 3.2, the systematic analysis of morphology and propagation of a crack in a transient network has been reported very recently in a single publication [Tabuteau et al (2011)]. The fracture propagation arising in pendant drop experiments has been tracked by high speed velocimetry [Tabuteau et al (2011)]. This configuration allows for an excellent reproducibility of the fracture initiation and propagation, as well as a pure elongational stress condition due to the lack of contact with solid interfaces near the fracture region. The fracture of the fluid happens in two steps. The fracture initiation step, reviewed in the previous paragraph and reported in [Tabuteau et al (2009a)] was shown to be governed by the thermally activated nucleation of a critical crack in the polymer network. The second step, consisting in the rapid propagation of a brittle fracture in the fluid, was analyzed in detail and shown to be energetically governed by the surface tension of the solvent (oil- in-water droplet microemulsion). Indeed, from the beginning of the propagation up to the complete fracture (i.e., when the sample is separated in two parts) the fracture profile exhibits a parabolic shape (Figure 9) as expected for an elastic solid breaking under tension [Irwin (1957)]. These observations were confirmed by quantitative analysis of the fracture profile $u(x)$ on the crack propagation across the sample (Figure 11).

Interestingly, the authors show that, because of the low value of the elastic modulus of the transient network, and as in soft solids [Seitz et al (2009)], the crack tip region exhibits very large deformations that require the use of finite elastic theories [Hui et al (2003)] for a proper description. The non-linear character of the problem requires the fracture energy to be estimated by the J-integral method [Rice (1968)] and the strain energy release $\mathscr{G}$ can be related to the curvature radius of the tip R_{tip} through $\mathscr{G} \approx J = \pi G_0 R_{tip}/2$. The brittle character of the fracture propagation is confirmed by the fact that the measured fracture energy is independent of crack velocity V and equal to the Dupré work, that is the reversible work needed to form two new air/gel surfaces $2\Gamma_s$ (dry fracture), without any bulk viscous dissipation. According to the viscoelastic trumpet model of de Gennes [de Gennes (1996)] applied to a Maxwell fluid [Saulnier et al (2004)], the absence of bulk viscous dissipation was justified by the short length L of the crack (less than the filament diameter) in relation to the characteristic length $V\tau$ above which the viscous dissipation starts to become effective (Figure12). An extension of the trumpet model to the hyper elastic case allows to confirm the weakness of the dissipated energy in terms of a new relevant length scale $R_{tip} \sim \mathscr{G}/G_0$, of the same order of magnitude as the observed crack lengths. In agreement with this interpretation, the measured crack opening profiles present a constant parabolic shape.

Despite the brittle character of the propagation, the authors report a slow velocity of crack propagation $V \approx$ mm/s $\ll c_R$, $c_R \approx \sqrt{G_0/\rho}$ on the order of 1m/s, being the speed of sound in the medium, expected for a brittle solid. The authors propose a microscopic model for thee scaling of the velocity V of the fracture to be governed by the time scales of the local crack tip debonding processes (Figure 13), and namely
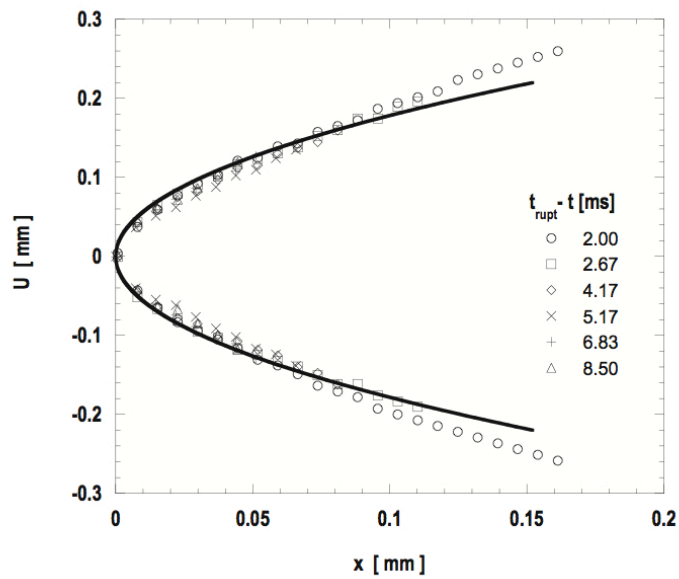
Fig. 11 From [Tabuteau et al (2011)]: Fracture profiles $u(x)$ for different times before the break-up in the fracture moving frame, corresponding to the pictures of figure 9. The black line is a parabolic fit corresponding to $u(x) = a\sqrt{(x)}$ with $J = \pi G_0 a^2 / 4$ and $J = 2\Gamma_s$. We report only the profile for $L < 0.1 D_0$
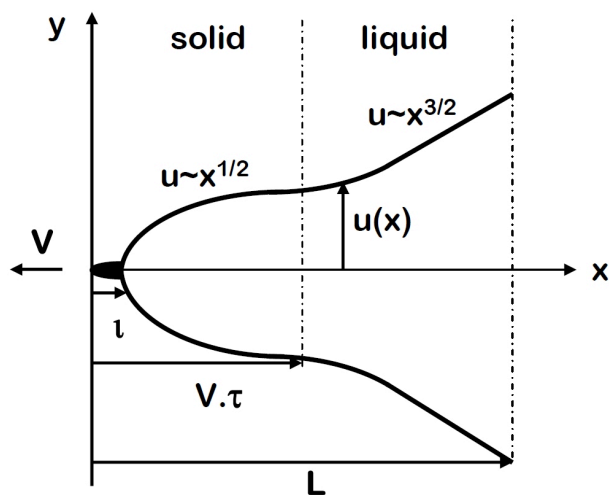
Fig. 12 From [Tabuteau et al (2011)]: A schematic representation of the space and time scales associated to a crack of length L moving with velocity V in a Maxwell fluid of relaxation time τ according to the trumpet model[de Gennes (1996)]. A small microscopic nonlinear zone of length l is represented in black. The behavior of the material is solid like at scales smaller than $V\tau$, then fluid like at larger scales, and accordingly the fracture profile scales differently with the distance to the crack's tip in the two different regions.
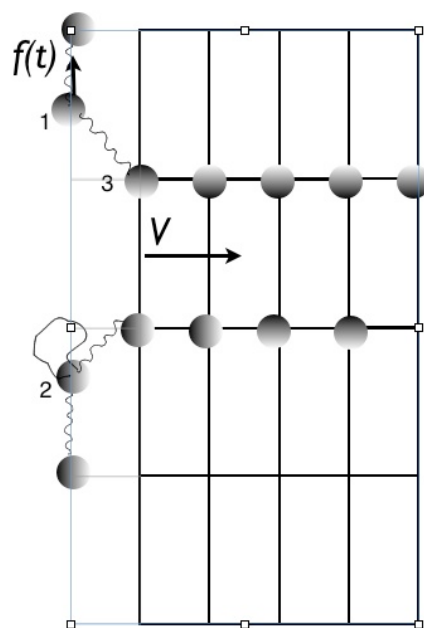
Fig. 13 From Ref [Tabuteau et al (2011)]: Cartoon of the viscous relaxation mechanism of a bead at the tip of the fracture. The polymer bridge between beads (1) and (2) just debonded, forming a loop on bead (2). Bead (1) thus experiences the spring-back force $f(t)$ due to the gel under tension; this will lead to an increasing extra tension on bead (3) and crack propagation at velocity V.

by the elastic relaxation time of the oil droplets after a debonding event under the action of the viscous drag of the solvent (Reynolds number $R_e \ll 1$). This leads to an upper limit for the estimation of the crack velocity $V \lesssim 0.25 \frac{G_0 \xi^2}{2\pi \eta_W b}$, where G_0 is the shear modulus of the gel, b the radius of the droplet and ξ the mesh size and η_W is the viscosity of water. The control of the crack velocity by network/solvent friction has been already observed by Baumberger *et al.* [Baumberger et al (2006b,a)] in the viscoplastic fracture dynamics of thermoreversible gels.

4 Brittle vs Ductile fractures

Ductility versus brittleness characterizes the nature of fracture mechanism in solids under stresses when irreversible damages take place. Brittle solids suddenly break in the elastic regime above a critical stress, whereas ductile solids plastically deform, before fracturing. Ductility implies that some specific mechanism exists, allowing local rearrangements and creeping while the micro-structure is on the average preserved. Speaking of brittle fractures for viscoelastic fluids seems a priori paradoxical since, like all liquids, they accommodate arbitrarily large deformations after a finite relaxation time: in that sense they are infinitely ductile. However, since the pioneering works of Vinogradov and coworkers in the 1970s and 1980s, it has been recognized

that polymers melt can fail either in a ductile or a brittle mode, as discussed in details in [Wang and Wang (2010); Boukany et al (2009)]. The switch of the failure mode from yielding to elastic rupture is controlled by the Rouse Weissenberg number.

The observation of fluid fractures in extensional geometry clearly reveals two distinct rupture scenari (elastic rupture versus necking and pinch-off) observed in viscoelastic fluids and reviewed in section 3.3, that are reminiscent of brittle versus ductile fracture behaviors observed in solid material. Interestingly, two transient networks (one consisting of cross-linked polymers the second of entangled living polymers [Dreiss (2007)], the other having the same simple Maxwell linear rheological behavior exhibit the two distinct different fracture behaviors as shown in pendant drop experiments [Tabuteau et al (2008)] (Figure 14). Intuitively, the fracture should occur when the material does not have enough time to relax, i.e. when the flow time scale is faster than the relaxation time. This condition is equivalent to the condition that the Deborah number is larger than 1 [Gladden and Belmonte (2007)]. However, as shown in Figure 14 and in [Tabuteau et al (2008)], this appealing simple picture is a bit too naive. Bhardwaj *et al* [Bhardwaj et al (2007)] observed both types of fracture in solutions of entangled micelles and suggested that the smooth pinch-off mode observed for the more concentrated sample might be the results of structural modifications of the solution of entangled wormlike micelles. On the other hand, Sprakel *et al* [Sprakel et al (2009b)] investigated flow failure modes for transient polymer networks using particle-based simulations and showed transition from shear banding to melt fracture upon changing the polymer concentration. Tixier *et al* [Tixier et al (2010)] reported the existence of a new class of self-assembled transient networks made of surfactant micelles of tunable morphology (from spheres, to rodlike to wormlike, Figure 15) reversibly linked by telechelic polymers, designed to achieve a comprehensive study of the brittle to ductile transition in self-assembled networks. Flow curves of the transient networks of tunable morphology suggest that one can associate three domains as the micelles growth with distinct failures modes: a brittle mode, an intermediate mode and finally a ductile/shear banding mode, as the micelles grow.

Coupling rheology and time-resolved structural measurements using synchrotron radiation [Ramos et al (2011)], Ramos and Ligoure show that the bridged micelles can align under shear and proposed the emergence of strong fluctuations of the degree of alignment of the micelles as a structural probe of a fracture process under shear (Figure16). The transition from a regime where the fluctuations of the are weak to a regime where the fluctuations are strong is rather sharp and enables to define a critical shear rate for the onset of strong fluctuations $\dot{\gamma}_{fracture}$. By analogy with solid materials, and mapping the strain in solids to the shear rate of viscoelastic fluids under shear, the authors therefore propose to compare the shear rate for the onset of fracture $\dot{\gamma}_{fracture}$ and the shear rate for the onset of non-linearity $\dot{\gamma}_{thin}$. They define Δ as the normalized difference between the two critical shear rates $\Delta = (\dot{\gamma}_{fracture} - \dot{\gamma}_{thin})/\dot{\gamma}_{thin}$. This parameter Δ is analogous o the amount of plastic deformation accumulated before fracture in ductile materials. So, the critical shear rate for fracture is either very close to the shear rate at which the sample departs from its linear behavior (for "brittle-like" samples) or significantly larger than the shear rate at which the sample departs from its linear behavior (for "ductile-like") samples, and the ability of
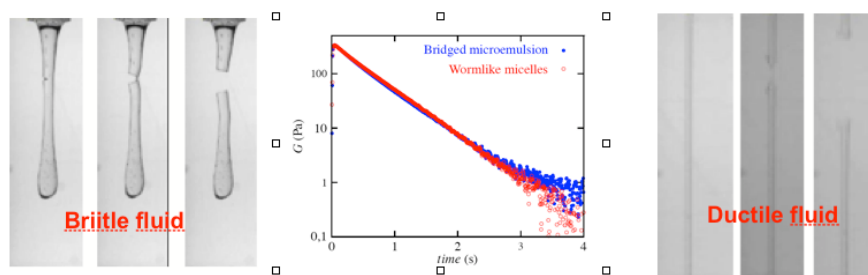
Fig. 14 From Ref [Tixier et al (2010)]: **Middle**: Shear stress relaxation function $G(t)$ for two model experimental systems of transient networks (bridged microemulsions and wormlike micelles). Both systems exhibit the same Maxwell behavior. **Left**: Fall of a droplet of the bridged microemulsion sample under the influence of gravity. Photographs taken at times (0, 10 ms, 20 ms) from the left to right. The diameter of the filament is $\approx$ 5 mm. **Right**: Fall of a droplet of a wormlike micelles sample under the influence of gravity. Photographs taken at times (0, 66 ms, 67 ms) from the left to right. The diameter of the filament is $\approx$2 mm.
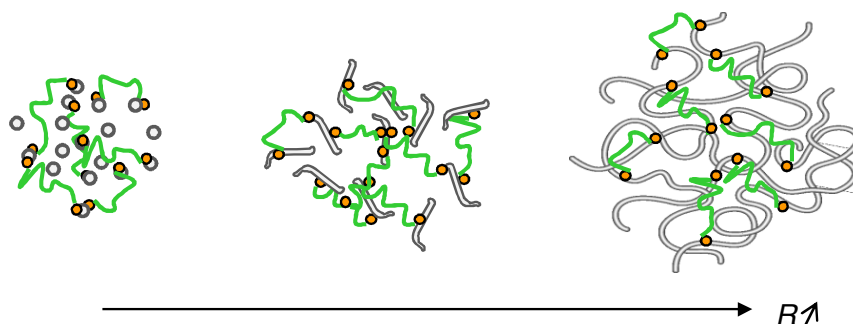
Fig. 15 From Ref [Tixier et al (2010)]: Schematic view of the structure of transient networks with nodes of tunable morphology. Upon variation of the co-surfactant to surfactant molar ratio of the micelles, the morphology of the nodes evolves from spherical (left) to rodlike (middle) to wormlike (right).

transient networks to exhibit a ductile-like behavior should be related to its ability to rearrange its structure at large scale under flow, before relaxing its elastic energy.

5 Theoretical approaches of crack nucleation in transient networks

Experiments reported by different groups on various transient networks but with similar structures and microscopic dynamical properties lead to several interpretations that do not seem at first glance compatible, leading to some confusion [Skrzeszewska et al (2010); Berret and Serero (2001); Tabuteau et al (2008, 2009a, 2011)]. Sections 5.2, 5.3 and 5.4 are devoted to theories for the nucleation of brittle fractures, and to the confrontation of these theories with experimental results. Section 5.2 deals with the *thermally activated crack nucleation model* (TAC model) [Golubovic and Feng (1991); Pomeau (1992)]. In section 5.3 *the activated bond rupture model* (ABR model) [Evans and Ritchie (1997); Chaudhury (1999); Skrzeszewska et al (2010)] is
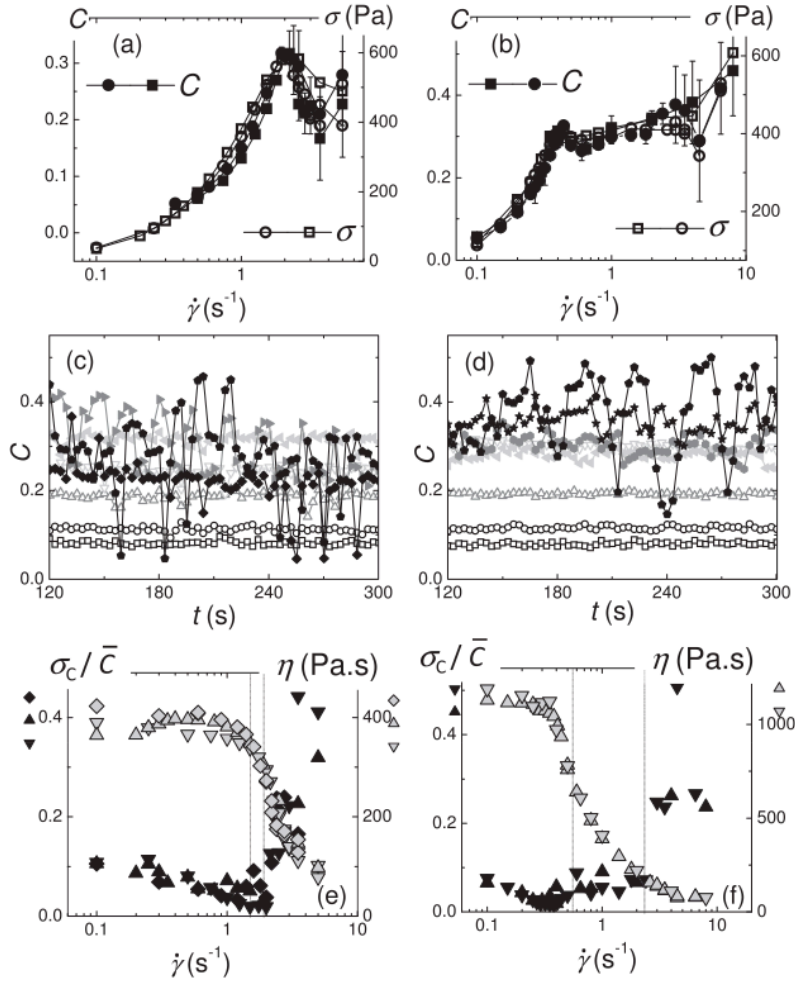
Fig. 16 From Ref [Ramos et al (2011)]: (a), (b): Shear stress (open symbols) and Contrast (full symbols) of the applied shear rate, $\dot{\gamma}$, in the steady state. The two sets of data in (a) and (b) correspond to two independent measurements. The bars for the contrast data correspond to the standard deviation. (c),(d): Time evolution of the contrast in the steady state as a function of $\dot{\gamma}$. (e),(f) Normalized fluctuations of the contrast (black symbols) and viscosity (gray symbols) as a function of $\dot{\gamma}$. (a), (c), (e): brittle fracture behavior; (b), (d), (f) ductile fracture behavior.

introduced. The starting point of these two models is the Griffith theory for fracture in brittle materials [Griffith (1921)], where a critical length for crack growth is expressed as a function of the applied load (Section 5.1). This length is reached by the thermal fluctuations in the TAC model, whereas it results of an acceleration in the rupture rate of the bonds near a crack tip in the ABR model. A third model, that we call *Self healing and activated bond rupture nucleation model* (SH-ABR model)[Mora (2011)] is introduced in section 5.4. It is based on the balance between cross-links

disconnection and reconnection [Mora (2011)] to control crack nucleation. Finally, the validity of these models is compared and discussed in section 5.5.

5.1 Griffith Fracture Criterion

The Griffith's theory for fracture in brittle materials [Griffith (1921)] starts up with preexisting micro-cracks and considers the energy required for them to grow spontaneously under a given constant stress. An interfacial energy has to be paid to break more cohesive bonds, counterbalanced by the bulk elastic energy released by the opening of the crack. For a given stress σ the Griffith free energy cost W for a crack of size L reads, in 3D:

$$W(\sigma, L) = \frac{\pi}{2} L^2 F_s - \alpha \frac{\pi L^3 \sigma^2}{2 G_0}, \tag{1}$$

with L the size of a disc-like crack, F_s the cohesive energy per unit area, G_0 is the shear modulus and $\alpha \simeq 1$ a constant depending on geometrical factors. A typical example of the Griffith potential as a function of L is shown on Figure 17. The stress σ being fixed, $W(\sigma, L)$ reaches a maximum:

$$W_{max}(\sigma) = \frac{6\pi}{\alpha^2} \frac{F_s^3 G_0^2}{\sigma^4} \tag{2}$$

for a crack size (the so called Griffith length)
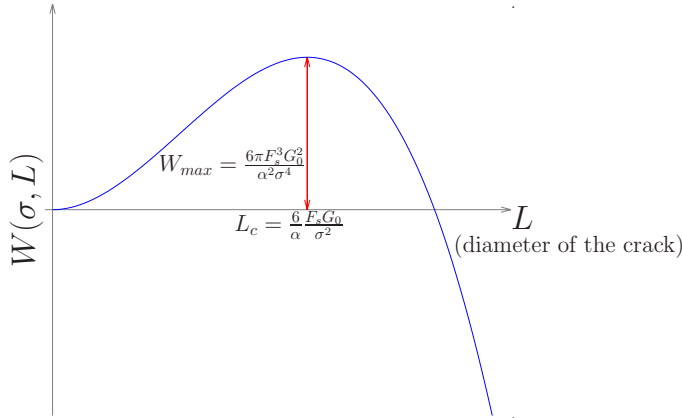
Fig. 17 Sketch of the Griffith's free energy of a crack as a function of the crack length L. Note that this curve can be scanned in both directions (increasing or decreasing L) for self-healing materials, in contrast with usual non-self-healing materials.

$$L_c(\sigma) = \frac{6}{\alpha} \frac{F_s G_0}{\sigma^2}. \tag{3}$$

For a crack size larger than $L_c, dW/dL < 0$, leading to a catastrophic growth of the crack (fracture), in contrast with a crack size smaller than L_c. Thus, a stressed sample appears to be in a metastable state as long as no crack with a size larger than L_c nucleates [Golubovic and Feng (1991); Pomeau (2002)].

5.2 Thermally activated crack nucleation model (TAC model)

A material submitted to a constant stress breaks after a given waiting time, that depends on the applied stress. Delayed fractures have been reported for a large variety of materials, ranging from 2d-microcrystals [Pauchard and Meunier (1993, 1998)] to heterogeneous materials [Guarino et al (1999); Ciliberto et al (2001); Guarino et al (2002)] and gels [Bonn et al (1998)]. More recently, experimental evidences of delayed fractures have been reported in transient networks [Tabuteau et al (2009a); Skrzeszewska et al (2010)] and a good agreement has been found with predictions of the TAC model [Pomeau (1992)], whose starting point is the Griffith theory. Several authors [Golubovic and Feng (1991); Pomeau (1992); Buchel and Sethna (1997); Pomeau (2002)] have proposed that the Griffith's energy (Eq. 1) is an energy barrier of height $W_{max}(\sigma)$. Then, the waiting t_1 should follow the Kramer's theory [Hanggi et al (1990)]:

$$\langle t_1 \rangle \propto exp\left(\frac{W_{max}(\sigma)}{k_B T}\right), \tag{4}$$

where $\langle . \rangle$ is for averaging over the stochastic distribution of fracture waiting times. The choice of an energy barrier implicitly assumes that a crack can reversibly explore states with different crack lengths between the initial and the critical ones.

A key characteristic of crack nucleation in transient networks is the intrinsic reversibility of the process. This directly comes from the transient nature of the junctions: new junctions can randomly appear between the two opposite sides of a crack. This is in fundamental contrast with what happens in non-self-healing materials, where the crack length irreversibly increases, making Eq. 4 irrelevant for solid materials. Recent models can overcome this specific difficulty of non-self-healing materials [Santucci et al (2003, 2007)].

A direct way to check predictions of the TA model is to measure the average fracture waiting time for different values the applied stress. Putting Eq. 2 in Eq. 4, one obtains:

$$\langle t_1 \rangle \simeq \tau_1 \exp\left[\left(\frac{\sigma_1}{\sigma}\right)^4\right], \tag{5}$$

where the prefactor τ_1 varies much more gently as a function of σ, than the exponential for $\sigma \gg \sigma_1$. The variation of the fracture waiting time given by Eq. 5 is very stiff when the stress is close to the characteristic stress σ_1: the waiting time becomes very long as soon as the stress decreases below σ_1, and becomes extremely short if the stress increases beyond σ_1. This sharp variation makes difficult the experimental determination of the waiting time variations with respect to the applied stress: the average waiting time should vary over several decades to check Eq. 5. Skrzeszewska et al. [Skrzeszewska et al (2010)] have measured the fracture waiting time for transient

polymer networks formed by telechelic polypeptides, with nodes made by the self association of three collagen-like triple helices [Skrzeszewska et al (2009)]. The sample is put in a rheometer equipped with a Couette geometry, and a given constant stress is applied. The measured waiting time t_b is defined as the elapsed duration between application of the stress and the instant when the measured shear rate jumps sharply by several decades (Figure 3). An important feature emerging from these experiments is the great dispersion for the measured values of the waiting times. This dispersion is inherent to the stochastic feature of the subcritical fracture. t_b is plotted in Figure 18 for different values the imposed constant stress. According to available data, the standard deviation reached one decade. t_b is plotted as a function of $(\sigma/G_0)^4$ (in semi-logscales, Figure 18-Left, G_0 being the shear modulus). Note that the data point corresponding to $\sigma/G_0 = 3$ comes from a strain versus time measurement whose appearance is significantly different from the others (smallest applied stress of Figure 3), which is a possible manifestation of the phenomenon of wall slipping at high stresses [de Gennes (2007); Erk et al (2012)]. However, even excluding this data point, the agreement between the experimental data and the prediction is not sufficiently clear to state that the TAC model provides an explanation for the existence of the observed delayed fracture as explained in section 5.3.
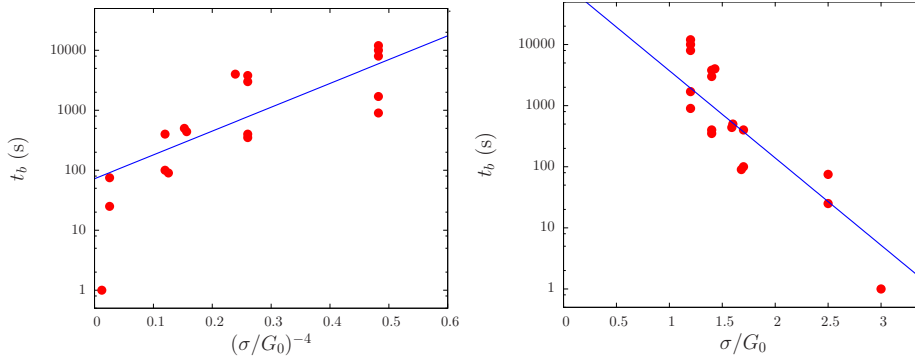
Fig. 18 Data from [Skrzeszewska et al (2010)]: Measured fracture waiting time (t_b) as a function of the applied stress. **Left**: t_b as a function of $(G_0/\sigma)^4$. The straight line represents the best fit for $t_0 \exp\left((\sigma_1/\sigma)^4\right)$ ($\sigma_1/G_0 = 1.74 \pm 0.08$). **Right**: representation in a semi-logarithmic scale. The straight line shows the best fit for an exponential decay $t_0 \exp(-\sigma/\sigma_2)$ ($\sigma_2/G_0 = 3.3 \pm 0.6$).

Another way to check a basic prediction coming from the TAC-model is to measure the characteristic value σ_1 of the stress and to compare it to the expression following the model. From Eqs.(2, 5) σ_1 reads:

$$\sigma_1 = \left(\frac{6\pi}{k_B T \alpha^2}\right)^{1/4} F_s^{3/4} G_0^{1/2}. \tag{6}$$

σ_1 can be interpreted as follows: the fracture propagation is subcritical for a load smaller than σ_1. Otherwise, the fracture nucleates instantaneously. σ_1 can be esti-

mated as follows. Let ξ be the typical mesh size of a transient network. Following Green and Tobolsky [Green and Tobolsky (1946)], the shear modulus is $G_0 \simeq ak_BT/\xi^3$, where a, of order unity, depends on the network topology. In order to estimate the value of F_s, we consider a micro-crack of the network. First of all it is important to note that micro-cracks in these networks are completely wet by the solvent and thus only the polymer network contributes to F_s (see Figure 19). The energy cost for creating a network-solvent interface originates from the depletion of the chains monomers at the crack interface. We use the well known analogy between transient networks and polymers solution in the semi-dilute regime: the cost in free energy per unit surface due to the depletion is [Joanny et al (1979)] $F_s \simeq a'\frac{k_BT}{\xi^2}$, where a', of order unity, also depends on the network topology. Then, Eq. 6 yields:

$$\sigma_1 \simeq \left(\frac{6\pi a'^3 a^2}{\alpha^2}\right)^{1/4} \frac{k_BT}{\xi^3} = \left(\frac{6\pi a'^3 a^2}{\alpha^2}\right)^{1/4} G_0. \tag{7}$$

The value of the prefactor being not far from unity, it appears that σ_1 is close to the shear modulus. Particle-based simulations where σ_1 is plotted versus polymer concentration corroborate Eq. 7 [Sprakel et al (2009b)]. Note that in Eq. 7, σ_1 is independent of the relaxation time and of the viscosity. It is therefore independent of the shear rate.

The best fit (Figure 18) of the data of Skrezesezewska et al. [Skrzeszewska et al (2010)] with Eq. 5 (excluding, as explained above the data point corresponding to $\sigma = 3G_0$), gives $\frac{\sigma_1}{G_0} \sim 1.74 \pm 0.08$, in agreement with Eq. 7.

Tabuteau et al. have measured σ_1 using pendant drop experiments, as introduced in section 3.3.2. The authors used a model system made of oil-in-water microemulsion droplets connected to each other by telechelic polymers (see Figure 19)[Filali et al (1999)] at different concentrations in order to vary both the relaxation time and the elastic modulus. In pendant drop experiments, the increase in stress with time is large enough to neglect the probability of breaking due to a subcritical fracture stress. Therefore the characteristic stress σ_1 in Eq. 7 is equal to the stress at the detachment in pendant drop experiments. The structure of this transient network being well characterized (particularly the network connectivity), it is possible to obtained an explicit expression for coefficients a and a' in Eq. 7 [Tabuteau et al (2009a)] for this specific material. The agreement between measured critical stresses and the theoretical prediction is satisfactory (Figure 10).

This result confirms the physical basis of the interfacial cohesive energy and allows the authors to conclude that the observed fractures are brittle. Note that the calculated value for the Griffith's length is, for all the samples, of the order of three times the mean distance between two oil droplets. This is consistent with the Griffith's theory. Furthermore, the measured critical stress has been found to be independent of the length of the stickers and therefore of the junction energy (note that the junction energy and the interfacial cohesive energy are here independent from each other). It is therefore independent of the transient network relaxation time [Tanaka and Edwards (1992e)]. This is consistent with the prediction of the the TAC-model for σ_1, where neither the junction energy nor the relaxation time do appear (see Eq. 7).

This last point is in contrast with the experiments of Skrezesezewska et al [Skrzeszewska et al (2010)] (see for instance Figure 20), showing that the TAC model fails -at least
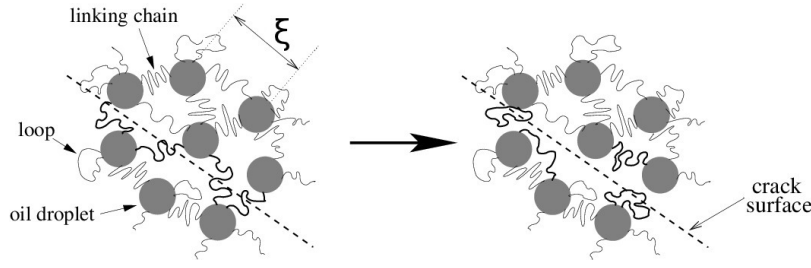
Fig. 19 Schematic of a bridged microemulsion. The telechelic polymers can either link two oil droplets or loop on a single one. (Left) Before the crack nucleation (bold dashed line) polymers can bridge oil droplets on both side of the bold dashed line. (Right) When the crack occurs, the same polymers cannot cross the bold dashed line anymore and form bridges in the other directions.

in part- for the experimental system used by these authors. This led them to focus on an alternative model, based on a more microscopic description of the phenomenon of fracture nucleation: the *activated bond rupture model* (ABR model).

5.3 Activated bond rupture model (ABR model)

Another way to describe fracture nucleation in transient networks is based on activated bond rupture [Evans and Ritchie (1997); Chaudhury (1999); Skrzeszewska et al (2010)].

In the systems we have in mind, the polymers are not entangled, so the single relevant time scale comes from the debonding kinetics. The free energy variation $\Delta \mathscr{G}_0$ characterizing a network junction is assumed to depend on the solvophobic length and the solvent quality. There is, by thermal fluctuations, a finite probability that a junction acquires sufficient energy to overcome the activation barrier $\Delta \mathscr{G}_0$ and detach spontaneously. Following the model of Green and Tobolsky [Green and Tobolsky (1946)], the exit rate $(1/\tau_0)$ is estimated as the product of a natural thermal vibration frequency, ν ($\sim 10^{10} - 10^{12}$ Hz) with $\exp\left(-\Delta \mathscr{G}_0 / k_B T\right)$. Hence, one expects

$$\frac{1}{\tau_0} = \nu \exp\left(-\frac{\Delta \mathscr{G}_0}{k_B T}\right). \tag{8}$$

From the Eyring kinetic theory of fracture [Eyring (1936); Kausch (1978)], Tanaka and Edwards [Tanaka and Edwards (1992b)] postulated that the lifetime of a junction also depends on the force carried by a link, whose stored energy can supply, through mechanical work, a portion of the activation energy. The junction lifetime τ becomes:

$$\tau = \frac{1}{\nu} \exp\left(\frac{(\Delta \mathscr{G}_0 - f\delta)}{k_B T}\right) = \tau_0 \exp\left(-\frac{f\delta}{k_B T}\right), \tag{9}$$

where f is the force carried by the link under tension, and δ a typical length on which the force works (for instance δ is the length of the solvophobic ends of telechelic polymers). A direct implication of this assumption is that a stretched bond breaks

more quickly than the non-stretched ones. Tanaka and Edwards predict the mechanical behavior of such transient networks under different conditions (strain oscillatory, transient, constant shear rate, etc.) [Tanaka and Edwards (1992b,c,d)]; they also predict non-linear effects (such as shear thinning) observed experimentally [Tam et al (1998); Ma and Cooper (2001); Sprakel et al (2008)]. These non-linearities come from the reduction of bond lifetime under load (Eq. 9). However, because this theory is itself a mean-field theory with affine deformations of the network junctions, the existence of a fracture completely escapes this model.

5.3.1 Constant load

If the length of a pre-existing crack is larger than the Griffith's length, then the fracture develops instantaneously, without delay. We are considering here, an opposite situation, where the crack size is smaller than the Griffith's length. The crack then grows slowly and can be described by the model of *the subcritical crack growth* [Santucci et al (2007)]. Because of the presence of heterogeneities due to thermal fluctuations in the network, the stress is inhomogeneous in the material, and then the force carried by a bond is not homogeneous. It is stronger where the bond density is low. Since the stress is concentrated near the crack tips, cross-links located just near a given tip will experience a higher force and then a higher dissociation rate. The kinetics of breakage is accelerated, which will result in a shorter time for the size of the micro-crack to reach the Griffith length. Once the crack reaches the Griffith length a catastrophic fracture follows. As a first approximation (i.e. neglecting the creation of new bonds), the average time $\langle t_2 \rangle$ required for the micro-crack to reach the Griffith length has to decrease exponentially with the applied stress [Brenner (1962); Zhurkov (1965)]:

$$\langle t_2 \rangle \sim \exp\left(-\frac{\sigma}{\sigma_2}\right), \tag{10}$$

where the characteristic stress σ_2 incorporates the factor $\delta/(k_B T)$ but also takes into account the stress concentration near the preexisting crack. Note that the σ^{-2}-variation of the Griffith length (Eq. 3) has been neglected because it varies much more slowly than the exponential.

Such dependence of the fracture waiting time (Eq. 10) as a function of the applied stress has been observed in several types of colloidal gels [Divoux et al (2010); Sprakel et al (2011)]. Skrzeszewska et al. [Skrzeszewska et al (2010)] have checked the validity of this approach for transient networks subjected to a constant load. They found a good agreement between Eq. 10 and their experimental data, as shown in Figure 18-Right. However, it is difficult to conclude from these data what is the relevant model among the TAC-model and the *activated bond rupture model* (ABR model); Indeed, none of the two plots of Figures 18 clearly prevails over the other.

Furthermore, the range of validity of Eq. 10 is limited, since cross-links re-formation are not taken into account. It can therefore be so inferred that this model cannot be applied for small loads, typically when the fracture waiting time $\langle t_2 \rangle$ exceeds the characteristic time of cross-links re-formations. In addition, Eq. 10 also predicts a

smooth variation without any abrupt jump for the fracture waiting time regardless of the value of the applied stress, contrary to other models (see sections 5.2 and 5.4 and Figure 23). This is in opposition with the existence of a experimentally observed fracture threshold (an unstressed transient network does not spontaneously break).

5.3.2 Constant shear rate

Sections 5.2 and 5.3.1 deal with crack nucleation for transient networks subjected to constant loads. In this case, the sample flows before breaking because the fracture does not appear instantaneously and because the material is a fluid. In this situation, the shear rate varies with time because it is subject to fluctuations even when the steady flow is still established.

Very commonly, a shear rate is imposed in rheological tests. Some studies have focused on fracture nucleation in a transient network subjected to a constant shear rate (see e.g. section 3.1.1) [Berret and Serero (2001); Skrzeszewska et al (2010)]. Skrzeszewska et al. [Skrzeszewska et al (2010)] observed that the failure stress and the waiting time (before the fracture occurs) depend on the imposed shear rate (Figure 20): the waiting time is found to decrease and the critical stress to increase as the constant shear rate is higher. Interestingly, the critical strain exhibits a non monotonic behavior on the share rate (Figure 20a), very similar as what is observed in uniaxial extension of polymeric liquids [Malkin and Petrie (1997)]. Particle-based simulations also show a weak but significant increase of the fracture stress with applied overall shear rate [Sprakel et al (2009b)]. The authors of [Skrzeszewska et al (2010)] have used the ABR model to explain these results. Within a mean field approximation, the deformation is affine and a bridging chain in the network is stretched at a speed $\xi \dot{\gamma}$, where $\dot{\gamma}$ is the (macroscopic) applied shear rate and ξ the typical distance between junctions. Supposing that bridging chains act as Gaussian chains with a spring constant $k_B T / \xi^2$, the force carried by a cross-link increases as $f(t) = K \frac{k_B T}{\xi} \dot{\gamma} t$, where the factor K accounts for the local stress enhancement in the vicinity of the crack tip [Skrzeszewska et al (2010)]. With Eq. 9 one obtains, for the survival probability of a bond $P(t)$ [Evans and Ritchie (1997)]:

$$P(t) = \exp \left\{ - \int_0^t \mathrm{d}t' \frac{1}{\tau_0} \exp \left(\frac{K k_B T \dot{\gamma} t' \delta}{\xi k_B T} \right) \right\}. \tag{11}$$

The average lifetime of a cross-link is

$$\langle \tau_0' \rangle = \int_0^\infty P(t) \mathrm{d}t. \tag{12}$$

In the high shear-rate limit, $\dot{\gamma} \tau \gg \frac{\xi}{K \delta}$ and $\dot{\gamma} \tau \gg 1$, re-formation of cross-links can be neglected. Eq. 12 simplifies and it follows that a fracture occurs after a time $t_2' \simeq \langle \tau_0' \rangle$

$$t_2' = \frac{\xi}{K \delta \dot{\gamma}} \ln \left(\frac{K \delta \dot{\gamma} \tau}{\xi} \right), \tag{13}$$

and the critical strain reads $\gamma_2' = \dot{\gamma} t_2' \simeq \frac{\xi}{K \delta} \ln \left(\frac{K \delta \dot{\gamma} \tau}{\xi} \right)$. Neglecting a possible strain hardening [Tabuteau et al (2009b); Serero et al (2000)], the stress at the rupture (σ_2')

can be estimated as $\sigma \simeq G_0 \gamma$. The experimental critical strain γ_2' is plotted in Figure 20-A for three different concentrations of a transient polymer networks formed by telechelic polypeptides (from [Skrzeszewska et al (2010)]). In order to make a more quantitative comparison between their experiments and the model, the authors have plotted dimensionless values of γ_2' and σ_2' ($\gamma_2'\delta/\xi^3$ and $\sigma_2'\delta/(G_0\xi)$) as a function of $\ln(\dot{\gamma}\tau\delta/\xi)$, where δ is the estimated length of a junction and ξ is estimated using $G_0 \simeq k_B T/\xi^3$. The curves superimpose with a nice agreement with theoretical predictions of Eq. 12 in the high shear limit. This gives a strong argument in favor of the relevance of the ABR model for this system, whereas the TAC-model predicts a shear rate independent failure stress. However, these predictions does not seem applicable to other transient networks, where a shear stress independent failure stress has been reported [Tabuteau et al (2009a)]. As explained below, the main weakness of the ABR model is that cross-links re-formations are neglected.
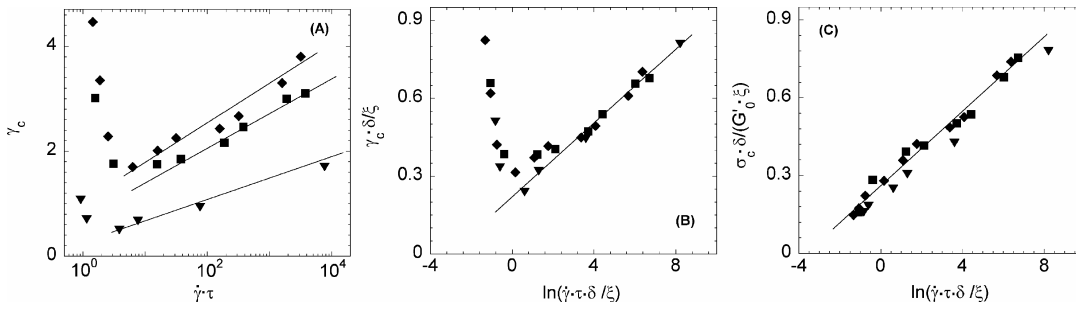
Fig. 20 From [Skrzeszewska et al (2010)]: A- Critical strain as a function of shear rate for transient polymer networks formed by telechelic polypeptides at different concentrations. Lines corresponds to the predictions of the ABR model. (B) Renormalized critical strain as a function of the logarithm of a renormalized shear rate, (C) Same for critical stress.

5.4 Self healing and activated bond rupture nucleation (SH-ABR model)

The fracture waiting time predicted by the ABR model leads to a finite waiting time whatever is the applied stress, even if it is zero. Following this prediction, an unstressed transient network should spontaneously break after a finite time. This inconsistency arises because the creation of new bonds (which could replace the broken bonds) is not taken into account. Recently, Mora [Mora (2011)] has proposed a model, the *Self healing and activated bond rupture nucleation model* (SH-ABR model), which aims to describe fracture nucleation in transient networks considering **both** activated bond rupture and cross-links re-formation to overcome the intrinsic limitation of the ABR model.

It is based on the fiber bundle model, usually used to study fracture in heterogeneous materials [Coleman (1958); Moreno et al (1999); Kun et al (2000); Ciliberto et al (2001); Pradhan et al (2010)]: a set of fibers (or bonds) is located on a supporting lattice and a random stress threshold is assigned to its elements. The set is loaded

and a bond breaks when its load exceeds a threshold value. In the equal load sharing hypothesis (or global), which is the simplest scheme one can suppose, it is assumed that the load carried by failed elements is equally distributed among the surviving elements of the system. The SH-ABR model deals with systems without entanglement. The relaxation time of a link is then assumed to be far shorter than the bonds lifetime.In this model, a bond just once broken becomes active again: It can either take back the place it had or bridge another junction. Mora [Mora (2011)] first considered a one dimensional model (see Figure 21) subjected at time $t = 0$ to an external stress σ. It is assumed that (i) following the Eyring kinetic theory of fracture [Eyring (1936); Kausch (1978); Tanaka and Edwards (1992a)], the lifetime τ is given by Eq. 9, and (ii) one end of a bond that has just escaped will reconnect over a much shorter duration than the (load depending) lifetime of a bond (as in most of experimental systems).
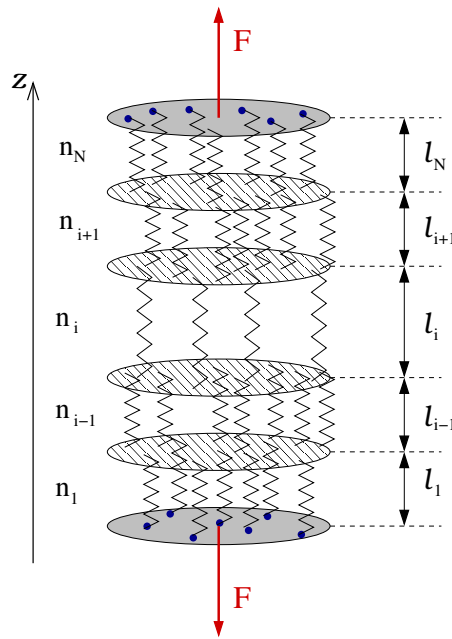
Fig. 21 From [Mora (2011)]: Schematic of the one-dimensional model. The system is composed of N layers. The layer number i is connected to the layer number $i + 1$ by n_i bonds. The total number of bonds and layers is fixed once and for all. All bonds are identical. They can connect only two adjacent layers. One end of a bond can migrate from one layer to another. A force applied to the ends is transmitted layer by layer. Within a layer, this force is split evenly between the springs.

An analytical critical magnitude of the applied stress is predicted in 1D:

$$\sigma_3 = \frac{n_0 \xi k_B T}{\delta},$$

(14)

where n_0 is the number of network junctions per unit volume and ξ the mesh size of the network (the distance between two layers in the one-dimensional model, see Figure 21). Beyond this threshold, any concentration inhomogeneity in the bonds distribution is amplified, leading to the formation and the catastrophic and irreversible growth of cracks. On the contrary, any inhomogeneity in the bonds distribution decreases in time when the applied stress is below this threshold value. Note that the load dependence of the bond lifetime (formally: $\delta \neq 0$ in Eq. 14) is here a necessary condition for the existence of a fracture stress threshold.

The time $\langle t_3 \rangle$ at which the concentration of bonds vanishes somewhere in the one-dimensional system is by definition the failure time. This time is found to depend on the ratio $\frac{n_0 \xi k_B T}{\sigma \delta}$ (Figure 22). It tends to infinity as $\frac{n_0 \xi k_B T}{\sigma \delta}$ tends to one *i.e.* when approaching the failure threshold ($\sigma = \sigma_3$). Of course, the failure time is not defined for $\frac{n_0 \xi k_B T}{\sigma \delta} > 1$.
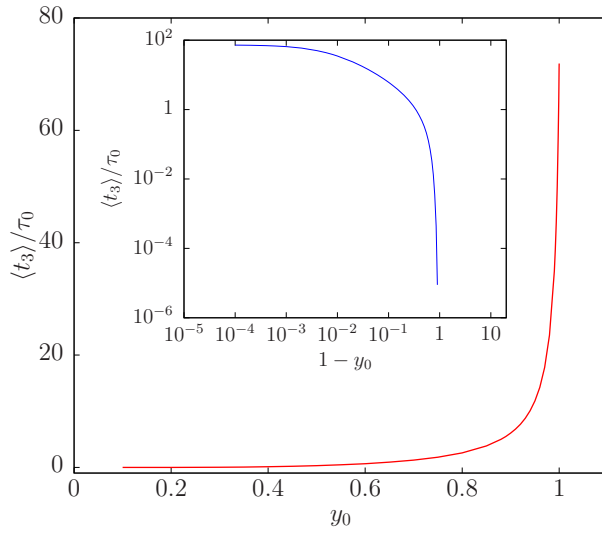
Fig. 22 From [Mora (2011)]: Reduced failure time t_3/τ_0 as a function of $y_0 = \frac{n_0 \xi k_B T}{\sigma \delta}$. This time diverges to infinity on approaching the rupture threshold. Insert: Same curve in logarithmic scales.

A similar result was found when the strain is imposed. The threshold value of the deformation beyond which rupture occurs is simply equal to the ratio of the critical stress (Eq. 14) with the elastic modulus of the system. The fracture waiting time is finite when the imposed strain is above this threshold. It decreases gradually as the imposed strain increases.

Numerical simulations are used to validate the results, at least semi-quantitatively, for two-dimensional networks [Mora (2011)]. Note that the fractures under a constant shear rate have so far not been studied within this model.

In conclusion, the introduction of a self-healing process in the ABR model leads to a true fracture stress threshold.

5.5 Ranges of validity and discussion

We have presented three models that lead to different predictions for the fracture waiting time and for the critical failure stress (see Figure 23).

When the applied stress is large, the average bond lifetime is very short (see Eq. 9) and the effects of cross-links re-formation become negligible. Here, *large* means $\exp(-f\delta/(k_B T)) \ll 1$, i.e. $\sigma \gg \sigma_3$ (where σ_3 is given by Eq. 14). Figure 23 shows that for $\sigma \gg \sigma_3$ the decay of the fracture waiting time as a function of the stress is exponential, in accordance with the prediction of the ABR model, i.e. $\langle t_3 \rangle \simeq \langle t_2 \rangle$. So in this limit, the ABR and the SH-ABR models lead to the same predictions.

In the opposite limit, where $\exp(-f\delta/(k_B T)) \lesssim 1$ or equivalently $\sigma \lesssim \sigma_3$, the effects coming from the load dependence of the cross-links lifetime are negligible (formally, $\delta = 0$ in Eq. 9). The ABR model is no longer valid because the cross-links re-formation events are important. In this case the SH-ABR model predicts the absence of fracture (because $\sigma < \sigma_3$). Within this limit, the TAC-model is the only one able to explain the origin of the experimentally observed fractures.

Because $\langle t_3 \rangle \to \infty$ (resp. 0) for $\sigma \to \sigma_3^-$ (resp. ∞) and $\langle t_1 \rangle \to \infty$ (resp. τ_1) for $\sigma \to 0$ (resp. ∞), $\langle t_1 \rangle$ is smaller (resp. larger) than $\langle t_3 \rangle$ for low (resp. high) stresses (Figure 23).

Let us suppose that the relevant model is the one which predicts the shortest fracture waiting time for a given value of the stress. If $\sigma_1 < \sigma_3$, then $\langle t_1 \rangle$ intersects $\langle t_3 \rangle$ for a stress larger than σ_1 (Figure 23-right). As a result, $\langle t_3 \rangle$ will be the relevant fracture waiting time for stresses for which $\langle t_1 \rangle$ is of order τ_1 (a molecular time, Eq. 5), in contradiction with the implicit hypothesis of a finite breaking time. In the opposite case, where $\sigma_1 > \sigma_3$ (Figure 23-left), $\langle t_1 \rangle$ intersects $\langle t_3 \rangle$ for a stress smaller than σ_1 for which $\langle t_1 \rangle$ is a priori far larger than τ_1. The SH-ABR model then predicts a macroscopic fracture waiting time smaller than $\langle t_1 \rangle$. It is so the relevant model in this case.

The TAC and SH-ABR models described above must be thought of as asymptotic models. For intermediate stresses a more complete description must take into account all the ingredients of both models to give a more refined transition between the TAC-model and the SH-ABR model.

The condition for which the SH-ABR model is likely to adequately describe the fracture waiting time is (i) $\sigma_1 > \sigma_3$ and (ii) the applied stress is greater than the crossover stress for $\langle t_1 \rangle$ and $\langle t_3 \rangle$. From Eq. 7 and 14 condition (i) yields:

$$\left(\frac{6\pi a'^3 a^2}{\alpha^2} \right)^{1/4} G_0 > \frac{n_0 \xi k_B T}{\delta} \simeq \frac{\xi}{\delta} G_0. \tag{15}$$

Eq. 15 leads to the approximate condition (omitting the prefactor of order unity):

$$\delta > \xi. \tag{16}$$

The TAC-model applies at any stress when $\sigma_3 > \sigma_1$, i.e. for $\xi \gg \delta$.

Let us come back to the two main experimental systems introduced above. In the experiments of Tabuteau et al. [Tabuteau et al (2008, 2009a)], the mean distance
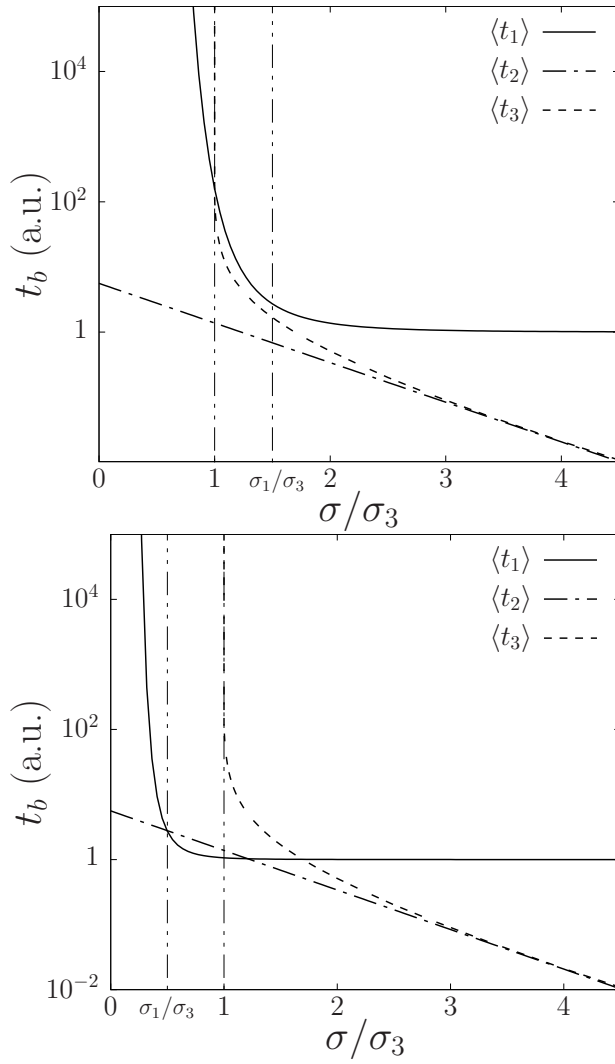
Fig. 23 Fracture waiting time t_b as a function of the applied stress calculated for the three models. Top: $\sigma_1 > \sigma_3$. In this case, the curves giving $\langle t_1 \rangle$ and $\langle t_3 \rangle$ intersect and the corresponding waiting time is not molecular ($t_b \gg \tau_1$). Bottom: $\sigma_3 > \sigma_1$. $\langle t_1 \rangle$ and $\langle t_3 \rangle$ intersect at a molecular time (τ_1 in Eq. 5).

between junctions is of the order of $\xi \sim 130$ *nm* whereas the length of a hydrophobic sticker is about $\delta \sim 10$ *mm*. Thus, $\delta/\xi \ll 1$ is consistent with the experimental measurements in agreement with the TAC-model.

Because the fine structure of the triple-helical junction in transient polymer networks formed by telechelic polypeptides as studied by Skrzeszewska is not well known, the estimation of δ/ξ is less accurate. The authors took $\delta \simeq 9$ *nm*, leading to a ratio δ/ξ ranging from 0.18 to 0.5, depending of protein concentration. This

limit corresponds to the situation where it is expected that the different models should be coupled. However, the experimental results obtained by the authors lead in favor of the ABR (or more SH-ABR) model. This suggests that the ABR model is preponderant even for values δ/ξ slightly below 1.

In summary, we have introduced three models, each of them predicting a fracture waiting time as a function of the applied load. We have assumed that the relevant model is the model predicting the shortest waiting time. Then, it is possible to predict the variation of the waiting time. The threshold values for the applicability of these models depend on (i) the value of the applied stress, and on (ii) the ratio δ/ξ.

6 Conclusion and Perspectives

Transient networks appear as simple model systems for the physicist to achieve a fundamental understanding of fracture phenomenons in complex fluids because of the unique transient character of the polymeric bonds; In this review we have focused on the specificities arising from the fluid and self-healing characters of these materials. Fractures of transient networks have been reported in several configurations: shear, extensional or hybrid geometries. The main results include:

• Experimental evidences of the occurrence of true fractures, that can be unambiguously distinguished from hydrodynamic instabilities in various geometries.

• Measurements of failure thresholds, expressed as the applied stress or the applied deformation (e.g. shear rate), and measurements of the fracture waiting time for subcritical stresses or deformations. Fracture waiting time as a function of the applied stress and threshold fracture stresses have been measured by different groups. These measurements have led to different conclusions in apparent contradiction. Different and somewhat contradictory theoretical approaches developed to understand the experiments have been reviewed. Two are emerging among them: the *Thermally activated crack nucleation model* (TAC model) and the *Self healing and activated bond rupture nucleation model* (SH-ABR model). Each model has a limited range of validity. Two characteristic lengths play a key role to discriminate between them: the average distance between two junctions of the network (ξ), and the size of the adhering part of the junctions (δ). For $\xi \gg \delta$, the TAC model is always relevant, whereas for $\xi \ll \delta$, the TAC-model is relevant for low applied stresses and the SH-ABR model is relevant for high stresses. This should explain the diversity of the experimental behaviors observed for different experimental systems.
An interesting challenge will be to formulate experimental systems for which the ratio δ/ξ can be finely tuned to check this hypothesis.

• Most of the experimental results and theoretical analysis have dealt situations where the lifetime of bonds is large with respect to the relaxation time of the polymeric linkers and so, dominates the systems response. This corresponds to brittle fractures: the understanding of the physics involved in nucleation and of brittle fractures begin to be clarified. The opposite situation where the relaxation of the polymeric linkers is comparable or larger than lifetime of the bonds is still poorly understood. Transient networks with polymer links in the entangled regime, or with nodes of tun-

able morphology, or near the percolation transition (marginal transient networks) will provide experimental realizations of this situation. From the theoretical side, this new time scale could be included in the SH-ABR model. This future direction will tackle dissipation mechanisms (viscous dissipation, structural reorganization, etc.) involved during nucleation of ductile fractures and during fracture propagation, to progress in the fundamental understanding of the concepts of brittleness and ductility in complex fluid.

• Finally, the role of the rigidity of the polymeric linkers in the fracture of transient networks is a big and challenging question to address in the future.

References

Ahn K, Osaki K (1995) Mechanism of shear thickening investigated by a transient network model. J Non-Newtonian Fluid Mech 56:267

Anna S, McKinley (2008) Effect of a controlled pre-deformation history on extensional viscosity of dilute polymer solutions. Rheol Acta 47:841–859

Anna S, McKinley G, DA N, Sridhar T, Muller J SJ ANS Huang, James D (2001) An interlaboratory comparison of measurements from filament-stretching rheometers using common test fluids. J Rheol 45:83–114

Annable T, Buscall R, Ettelaie R, Whittlestone D (1993) The rheology of solutions of associating polymers: Comparison of experimental behavior with transient network theory. J Rheology 37:695

Appell J, Porte G, Rawiso M (1998) Interactions between nonionic surfactant micelles introduced by a telechelic polymer. a small angle neutron scattering study. Langmuir 14:4409

BaggerJorgensen H, Coppola L, Thuresson K, Olsson U, Mortensen K (1997) Phase behavior, microstructure, and dynamics in a nonionic microemulsion on addition of hydrophobically end-capped poly(ethylene oxide). Langmuir 13:4204

Barenblatt G (1962) The mathematical theory of equilibrium cracks in brittle fracture. Adv in Appl Mech 7:55–129

Baumberger T, Ronsin O (2009) From thermally activated to viscosity controlled fracture of biopolymer hydrogels. J Chem Phys 130:061,102

Baumberger T, Ronsin O (2010a) A convective instability mechanism for quasistatic crack branching in a hydrogel. Eur Phys J E 31:51

Baumberger T, Ronsin O (2010b) Cooperative effect of stress and ion displacement on the dynamics of cross-link unzipping and rupture of alginate gels. Biomacromolecules 11:1571

Baumberger T, Caroli C, Martina D (2006a) Fracture of a biopolymer gel as a viscoplastic disentanglement process. Eur Phys J E 21:81

Baumberger T, Caroli C, Martina D (2006b) Solvent control of crack dynamics in a reversible hydrogel. Nat Mat 5:552

Bensimon D, Kadanoff LP, Liang S, Shraiman BI, Tang C (1986) Viscous flows in two dimensions. Rev Modern Phys 58:958

Berret JF, Serero Y (2001) Evidence of shear-induced fluid fracture in telechelic polymer networks. Phys Rev Lett 87:048,303

Berret JF, Calvet D, Collet A, Viguier M (1997) Fluorocarbon associative polymers. Curr Opin Colloid Interface Sci 2:424

Besseling R, Isa L, Ballesta P, Petekidis G, Cates ME, Poon WCK (2010) Shear banding and flow-concentration coupling in colloidal glasses. Phys Rev Lett 105:268,301

Bhardwaj A, Miller E, Rothstein JP (2007) Filament stretching and capillary breakup extensional rheometry measurements of viscoelastic wormlike micelle solutions. J Rheology 51:693

Bonn D, Kellay H, Ben-Djemiaa K, Meunier J (1998) Delayed fracture of an inhomogeneous soft solid. Science 280:265

Boukany PE, Wang SQ (2007) Use of particle-tracking velocimetry and flow birefringence to study nonlinear flow behavior of entangled wormlike micellar solution: From wall slip, bulk disentanglement to chain scission. Macromolecules 41:1455

Boukany PE, Wang SQ, Wang X (2009) Step shear of entangled linear polymer melts: New experimental evidence for elastic yielding. Macromolecules 42:6261

Brenner S (1962) Mechanical behavior of sapphire whiskers at elevated temperatures. Jour Appl Phys 33:33

van den Brule BHAA, Hoogerbrugge PJ (2000) Brownian dynamics simulations of reversible polymeric networks. J Non-Newtonian Fluid Mech 60:303

Buchel A, Sethna J (1997) Statistical mechanics of cracks: Fluctuations, breakdown, and asymptotics of elastic theory. Phys Rev E 55:7669–7690

Buehler MJ (2010) Colloqium: Failure of molecules, bones and the earth itself. Rev Mod Phys 82:1459

Chassenieux C, Nicolai T, LBenyahia (2011) Rheology of associative polymer solutions. Curr Opin Colloid Interface Sci 16:18

Chaudhury MK (1999) Rate-dependent fracture at adhesive interface. J Phys Chem B 103:6562

Ciliberto S, Guarino A, Scorretti R (2001) The effect of disorder on the fracture nucleation process. Physica D 158:83–104

Coleman B (1958) Statistics and time dependence of mechanical breakdown in fibers. Journal of Applied Physics 29:968–983

Considère A (1885) Mémoire sur l'emploi du fer et de l'acier dans les constructions. Annales des Ponts et Chaussées 9:574

Cordier P, Tournhilac F, Soulié-Zakovich C, LLeibler (2008) Self-healing and thermoreversible rubber from supramolecular assembly. Nature 451:0669

Divoux T, Tamarii D, Barentin C, Manneville S (2010) Transient shear banding in a simple yield stress fluid. Phys Rev Lett 104:208,301

Dreiss C (2007) Wormlike micelles: where do we stand? recent developments, linear rheology and scattering techniques. Soft Matter 3:956–970

Eggers J (1997) Nonlinear dynamics and breakup of free-surface flows. Rev Mod Phys 69:865

Eggers J, Villermaux E (2008) Physics of liquid jets. Rep Prog Phys 71:036,601

Erk K, Martin J, HU Y, Shull K (2012) Extreme strain localization and sliding friction in physically associating polymer gels. Langmuir 28(9):4472–4478

Evans E, Ritchie K (1997) Dynamic strength of molecular adhesion bonds. Biophys J 72:1541

Eyring H (1936) Viscosity, plasticity, and diffusion as examples of absolute reaction rates. Journal of Chemical Physics 4(4):283–291

Feder HJ, Feder J (1991) Self-organized criticality in a stick-slip process. Phys Rev Lett 66:2669

Fielding SM (2007) Complex dynamics of shear banded flows. SoftMatter 3:1262

Fielding SM (2011) Criterion for extensional necking instability in polymeric fluids. Phys Rev Lett 107:258,301

Filali M, Aznard R, Svensson M, Porte G, Appell J (1999) Swollen micelles plus hydrophobically modified hydrosoluble polymers in aqueous solutions: Decoration versus bridging. a small angle neutron scattering study. J Phys Chem B 103:7293

Filali M, Ouazzani M, Michel E, Aznard R, Porte G, Appell J (2001) Robust phase behavior of model transient networks. J Phys Chem B 105:10,528

de Gennes PG (1996) Soft adhesives. Langmuir 12:4497–4500

de Gennes PG (2007) Melt fracture of entangled polymers. European Physical Journal E 23(1):3–5

Gladden TR, Belmonte A (2007) Motion of a viscoelastic micellar fluid around a cylinder: Flow and fracture. Phys Rev Lett 98:224,501

Golubovic L, Feng S (1991) Rate of microcrack nucleation. Phys Rev A 43:5223–5227

Green M, Tobolsky A (1946) A new approach to the theory of relaxing polymer media. J Chem Phys 14:80

Greenwood J, Johnson K (1981) The mechanics of adhesion of visocelastic solids. Philos; mag A 43:697

Greffier O, kahwaji AA, Rouch J, Kellay H (1998) Observation of a finite-time singularity in needle propagation in hele-shaw cells. Phys Rev Lett 91:3860

Griffith AA (1921) The phenomena of rupture and flow in solids. Phil Trans Roy Soc London A221:163–198

Guarino A, Ciliberto S, Garcimartin A (1999) Failure time and microcrack nucleation. Europhysics Letters 47:456–461

Guarino A, Ciliberto S, Garcimartin A, Zei M, Scorretti R (2002) Failure time and critical behaviour of fracture precursors in heterogeneous materials. Eur Phys J B 26:141–151

Hanggi P, Talkner P, Borkovec M (1990) Reaction-rate theory - 50 years after kramers. Reviews of Modern Physics 62(2):251–341

Helgeson ME, Moran SE, Han HZ, Doyle PS (2012) Mesoporous organohydrogels from thermogelling photocrosslinkable nanoemulsions. NatureMaterials 11:344–352

Hernandez-Cifre G, Barenbrug T, Schieber JD, van den Brule BAA (2003) Brownian dynamics simulation of reversible polymer networks under shear using a non-interacting dumbbell model. J Non-Newtonian Fluid Mech 113:73

Hough L, Ou-Yang H (2006) Viscoelasticity of aqueous telechelic poly(ethylene oxide) solutions: relaxation and structure. Phys Rev E 73:031,802

Hui CY, Jagota A, Bennison SJ, Londono JD (2003) Crack blunting and the strength of soft elastic solids. Proc Royal Soc Lond A 459:1489–1516

Hutton JF (1963) Fractures of liquids in shear. Nature 200:646

Ide Y, White J (1976) The spinnability of polymer fluid filaments. J Appl Polym Sci 20:2511

Ide Y, White J (1977) Investigation of failure during elonga- tional flow of polymer melts. J Non-Newton FLui Mech 2:281–298

Ide Y, White J (1978) Experimental study of elongational flow and failure of polymer melts. J Appl Polym Sci 22:1061

Ignés-Mullol J, Zhao H, Maher JV (1995) Velocity fluctuations of fracture like disruptions of associating polymer solutions. Phys Rev E 51:1338

Irwin GR (1957) Analysis of stresses and strains near the end of a crack traversing a plate. Journal of Applied Mechanics 24:361–364

Joanny J, Leibler L, de Gennes P (1979) Effects of polymer solutions on colloid stability. Polymer Physics 17(6):1073–1084

Joshi YM, Denn MM (2004) Rupture of entangled polymeric liquids in elongational flow with dissipation. J Rheol 48:591

Kausch H (1978) Polymer Fracture. Springer-Verlag, Berlin

Kim B, Mooney D (1998) Engineering smooth muscle tissue with a predefined structure. Journal of biomedical materials research 41:322

Kim J, Kim S, Kim K, Jin Y, Hong S, Hwang S, Cho B, Shin D, Im S (2004) Applications of telechelic polymers as compatibilizers and stabilizers in polymer blends and inorganic/organic nanohybrids. Polymer 45:9071

Kun F, Zapperi S, Herrmann H (2000) Dammage in fiber bundle models. Eur Phys Jour B 17:269–279

Larson RG (1999) Structure and rheology of complex fluids. Oxford University Press, New-York

Lee J, Gustin J, Chen T, Payne G, Raghavan S (2005) Vesicle?biopolymer gels: Networks of surfactant vesicles connected by associating biopolymers. Langmuir 21:26

Lemaire E, Levitz P, Daccord G, van Damme H (1991) From viscous fingering to viscoelastic fracturing in colloidal fluids. Phys Rev Lett 67:2009

Livne A, Cohen G, Finberg J (2005) Universality and hysteretic dynamics in rapid fracture. Phys Rev Lett 94:224,301

Livne A, Ben-David O, Fineberg J (2007) Oscillations in rapid fracture. Phys Rev Lett 98:124,301

Lodge T, Taribajil R, Yoshida T, Hillmyer M (2007) Sans evidence for the crosslinking of wormlike micelles by a model hydrophobically modified polymer. Macromolecules 40:4728

Ma S, Cooper S (2001) Shear thickening in aqueous solutions of hydrocarbon endcapped poly(ethylene oxide). Macromolecules 34(10):3294–3301

Malkin AY, Petrie CJS (1997) Some conditions for rupture of polymeric liquids in extension. J Rheol 41:1

Manneville S (2008) Recent experimental probes of shear banding. Rheol Actal 47:301

Marrucci G, Bhargava S, Cooper S (1993) Models of shear thickening behaviour in physically cross-linked networks. Macromolecules 26:6483

McKinley GH, Sridhar T (2002) Filament-stretching rheometry of complex fluids. Annu Rev Fluid Mech 34:375

Meeker SP, Bonnecaze RT, Cloitre M (2004) Slip and flow in soft particle pastes. Phys Rev Lett 92:198,302

Meng X, Russel W (2006) Rheology of telechelic associative polymers in aqueous solutions. J Rheology 50:1989

Mewis J, Kaffashi B, Vermant J, Butera R (2001) Determining relaxation modes in flowing associative polymers using superposition flows. Macromolecules 34:1376

Michel E, Filali M, Aznar R, Porte G, Appell J (2000) Percolation in a model transient network: Rheology and dynamic light scattering. Langmuir 16:8702

Molino F, Appell J, Filalli M, Michel E, Porte G, Mora S, Sunyer S (2000) A transient network of telechelic polymers and microspheres: structure and rheology. J Phys Cond Matt 12:A491

Mora S (2011) The kinetic approach to fracture in transient networks. Soft Matter 7:4908

Mora S, Manna M (2009) Saffman-taylor instability for generalized newtonian fluids. Phys Rev E 80:016,308

Mora S, Manna M (2010) Saffman-taylor instability of viscoelastic fluids: From viscous fingering to elastic fractures. Phys Rev E 81:026,305

Mora S, Manna M (2012) From viscous fingering to elastic instabilities. Journal of Non-Newtonian Fluid Mechanics 173-174:30–39

Moreno Y, Gomez J, Pacheco A (1999) Self-organized criticality in a fibre-bundle-type model. Physica A 274:400–409

Nakaya-Yaegashi K, Ramos L, Tabuteau H, Ligoure C (2008) Linear viscoelasticity of entangled wormlike micelles bridged by telechelic polymers: An experimental model for a double transient network. J Rheology 52:359

Odenwald M, Eicke H, Meier W (1995) Transient networks by aba triblock copolymers and microemulsions: a rheological study. Macromolecules 28:5074

Olmsted P (2008) Perspectives on shear banding in complex fluids. Rheol Acta 47:283

Olsson U, Börjesson J, Angelico R, Ceglie A, Palazzo G (2010) Slow dynamics of wormlike micelles. Soft Matter 6:1769–1777

Otsubo B (1999) A nonlinear elastic model for shear thickening of suspensions flocculated by reversible bridging. Langmuir 15:1960

Pauchard L, Meunier J (1993) Instantaneous and time-lag breaking of a 2-dimensional solid rod under a bending stress. Phys Rev Lett 70:3565–3568

Pauchard L, Meunier J (1998) Experimental study of the breakage of a two-dimensional crystal. Phil Mag B 78:221–224

Pellens L, Ahn K, Lee S, Mewis J (2004a) Evaluation of a transient network model for telechelic associative polymers. J Non-Newtonian Fluid Mech 12:87

Pellens L, Gamez-Corrales R, Mewis J (2004b) General non linear rheological behavior of associative polymers. J Rheology 48:379

Petrie CSJ (2009) Considère reconsidered: Necking of polymeric liquids. Chemical Engineering Science 64:4693

Pomeau Y (1992) Brisure spontanée de cristaux bidimensionnels courbés. C R Acad Sci Ser 314:553

Pomeau Y (2002) Fundamental problems in brittle fracture: unstable cracks and delayed breaking. C R Mecanique 330:249–257

Pradhan S, Hansen A, Chakrabarti B (2010) Failure processes in elastic fiber bundles. Rev Mod Phys 82:499–555

Ramos L, Ligoure C (2007) Structure of a new type of transient network: Entangled wormlike micelles bridged by telechelic polymers. Macromolecules 40:1248

Ramos L, Laperrousaz A, Dieudonné P, Ligoure C (2011) Structural signature of a brittel-to-ductile transition in self-assembled networks. Phys Rev Lett 107:148,302

Renardy M (2004) Self similar breakup of non-newtonian fluid jets. In: Binding, DM, Walters, K (Eds), Rheology Reviews 2004 British Society of Rheology, p 171

Rice J (1968) A path independent integral and the approximate analysis of strain concentration by notches and cracks. J Appl Mech 35:379–386

Rothstein JP (2003) Transient extensional rheology of wormlike micelle solutions. J Rheol 47:1127

Santucci S, Vanel L, Guarino A, Scorretti R, Ciliberto S (2003) Thermal activation of rupture and slow crack growth in a model of homogeneous brittle materials. Europhysics Letters 62:320–326

Santucci S, Vanel L, Ciliberto S (2007) Slow crack growth: Models and experiments. Eur Phys J Special Topics 146:341

Saulnier F, Ondarçuhu T, Aradian A, Raphael E (2004) Adhesion between a viscoelastic material and a solid surface. Macromolecules 37:1067–1075

Seitz M, Burghardt W, Faber K, Shull K (2006) Self-assembly and stress relaxation in acrylic triblock copolymer gels. Macromolecules 40:1218

Seitz ME, Martina D, Baumberger T, Krishnan VR, Hui C, Shull K (2009) Fracture and large strain behavior of self-assembled triblock copolymer gels. Soft Matter 5:447

Semenov A, Joanny J, Khokhlov A (1995) Associating polymers: Equilibrium and linear viscoelasticity. Macromolecules 28:1066

Serero Y, Jacobsen V, Berret JF (2000) Evidence of nonlinear chain stretching in the rheology of transient networks. Macromolecules 33:1841

Skrzeszewska P, Sprakel J, de Wolf F, Fokkink R, Stuart MC, van der Gucht J (2010) Fracture and self-healing in a well-defined self-assembled polymer network. Macromolecules 43:3542

Skrzeszewska PJ, de Wolf A F, Werten MWT, Moers APH, Cohen Stuart MA, van der Gucht J (2009) Physical gels of telechelic triblock copolymers with precisely defined junction multiplicity. Soft Matter 5:2057–2062

Smolka LB, Belmonte A (2003) Drop pinch-off and filament dynamics of wormlike micellar fluids. J Non-Newtonian Fluid Mech 115:1

Spenley NA, Cates ME, McLeish TCB (1993) Non linear rheology of wormlike micelles. Phys Rev Lett 71:939

Sprakel J, Besseling NAM, Leermakers FAM, Cohen-Stuart MA (2007) Equilibrium capillary forces with atomic force microscopy. Phys Rev Lett 99:104,504

Sprakel J, Bartscherer E, Hoffmann G, Cohen Stuart MA, van der Gucht J (2008) Dynamics of polymer bridge formation and disruption. Phys Rev E 78:040,802

Sprakel J, Spruijt E, Cohen-Stuart MA, Michels MAJ, van der Gucht J (2009a) Intermittent dynamics in transient polymer networks under shear: Signs of self-organized criticality. Phys Rev E 79:056,306

Sprakel J, Spruijt E, van der Gucht J, Padding JT, Briels WJ (2009b) Failure-mode transition in transient polymer networks with particle-based simulations. Soft Matter 5:4748

Sprakel J, Lindström S, Kodger TE, Weitz DA (2011) Stress enhancement in the delayed yielding of colloidal gels. Phys Rev Lett 106:248,303

Sutter M, Siepmann J, Hennink W, Jiskoot W (2007) Recombinant gelatin hydrogels for the sustained release of proteins. Journal of Controlled Release 119:301

Tabuteau H, Mora S, Ramos L, Porte G, Ligoure C (2008) Ductility versus brittleness in self-assembled transient networks. Prog Theoretical Phys Supplement 175:47

Tabuteau H, Mora S, Porte G, Abkarian M, Ligoure C (2009a) Microscopic mechanisms of the brittleness of viscoelastic fluids. Phys Rev Lett 102:155,501

Tabuteau H, Ramos L, Nakaya-Yaegashi K, Imai M, Ligoure C (2009b) Nonlinear rheology of surfactant wormlike micelles bridged by telechelic polymers. Langmuir 25:2467–2472

Tabuteau H, Mora S, Ciccotti M, Hui CY, Ligoure C (2011) Propagation of a brittle fracture in a viscoelastic fluid. SoftMatter 7:9474

Tam K, Jenkins R, Winnik M, Bassett D (1998) A structural model of hydrophobically modified urethane-ethoxylate (heur) associative polymers in shear flows. Macromolecules 31(13):4149–4159

Tanaka F, Edwards S (1992a) Viscoelastic properties of physically cross-linked networks - transient network theory. Macromolecules 25:1516–1523

Tanaka F, Edwards S (1992b) Viscoelastic properties of physically cross-linked networks part 1. nonlinear stationary viscoelasticity. Non-Newtonian Fluid Mech 43:247–271

Tanaka F, Edwards S (1992c) Viscoelastic properties of physically cross-linked networks part 2. dynamic mechanical moduli. Non-Newtonian Fluid Mech 43:273–288

Tanaka F, Edwards S (1992d) Viscoelastic properties of physically cross-linked networks part 3. time dependent phenomena. Non-Newtonian Fluid Mech 43:289–309

Tanaka F, Edwards S (1992e) Viscoelastic properties of physically cross-linked networks-transient network theory. Macromolecules 25:1516

Tanaka Y, Fukao K, Miyamoto Y (2000) Fracture energy of gels. Eur Phys J E 3:395

Tirtaatmajda V, Jenkins R (1997) Superposition of oscillations on steady shear flow as technique for investigating the structure of associative polymers. Macromolecules 30:1426

Tixier T, Tabuteau H, Carrière A, Ramos L, Ligoure C (2010) Transition from brittle to ductile rheological behavior by tuning the morphology of self-assembled networks. Soft Matter 6:2699

Tripathi A, Tam KC, McInley GH (2006) Rheology and dynamics of associative polymers in shear and extension: theory and experiments. Macromolecules 39:1981

Vaccaro A, Marrucci G (2000) A model for the nonlinear rheology of associating polymers. J Non-Newtonian Fluid Mech 92:261

Vlad D, Ignés-Mullol J, Maher J (1999) Velocity-jump instabilities in hele-shaw flow of associating polymer solutions. Phys Rev E 60:4423

Wang Y, Wang SQ (2010) Rupture in rapid uniaxial extension of linear entangled melts. Rheol Acta 49:1179

Warriner H, Davidson P, Slack N, Schelhorn M, Eiselt M, idziak P, Schmidt H, Safinya C (1997) Lamellar biogels comprising fluid membranes with a newly synthesized class of polyethylene glycol-surfactants. J Chem Phys 107:3707

Werten M, Teles H, Moers A, Wolbert E, Sprakel J, Eggink G, de Wolf F (2009) Precision gels from collagen-inspired triblock copolymers. Biomacromolecules 10:1106

Winnik M, Yekta A (1997) Associative polymers in solution. Curr Opin Colloid Interface Sci 2:424

Xu B, Yekta A, Li L, Masoumi Z, Winnik M (1996) The functionality of associative polymer networks: The association behavior of hydrophobically modified urethane-ethoxylate (heur) associative polymers in aqueous solution. Colloids Surf A: Physicochem Eng Aspects 112:239

Yamamoto M (1956) The visco-elastic properties of network structure. 1 general formalism. J Phys Soc Japan 11:413

Zhao H, Maher JV (1993) Associating-polymer effects in hele-shaw experiments. Phys Rev E 47:4278

Zhurkov SN (1965) Kinetic concept of strength of solids. Int J Fract Mech 1:311